THE JOURNAL OF PHYSICAL CHEMISTRY B
A JOURNAL OF THE AMERICAN CHEMICAL SOCIETY

pubs.acs.org/JPCB

Article

Direct Observation of Cholesterol Dimers and Tetramers in Lipid Bilayers

Matthew R. Elkins, Asanga Bandara, George A. Pantelopulos, John E. Straub,* and Mei Hong*

Cite This: https://dx.doi.org/10.1021/acs.jpcb.0c10631

Read Online

ABSTRACT: Cholesterol is a ubiquitous component of mammalian cell membranes and affects membrane protein function. Although cholesterol-mediated formation of ordered membrane domains has been extensively studied, molecular-level structural information about cholesterol self-association has been absent. Here, we combine solid-state nuclear magnetic resonance (NMR) spectroscopy with all-atom molecular dynamics simulations to determine the oligomeric structure of cholesterol in phospholipid bilayers. Two-dimensional $^{13}C-^{13}C$ correlation spectra of differentially labeled cholesterol indicate that cholesterol self-associates in a face-to-face fashion at membrane concentrations from 17 to 44 mol %. 2D ^{13}C and ^{19}F spin-counting experiments allowed us to measure the average oligomeric number of these cholesterol clusters. At low cholesterol concentrations of ~20%, the average cluster size is centered on dimers. At a high cholesterol concentration of 44%, which is representative of virus lipid envelopes and liquid-ordered domains of cell membranes, both dimers and tetramers are observed. The cholesterol dimers are found in both phase-separated membranes that contain sphingomyelin and in disordered and miscible membranes that are free of sphingomyelin. Molecular dynamics simulations support these experimental observations and moreover provide the lifetimes, stabilities, distributions, and structures of these nanoscopic cholesterol clusters. Taken together, these NMR and MD data strongly suggest that dimers are the basic structural unit of cholesterol in phospholipid bilayers. The direct observation of cholesterol dimers and tetramers provides a revised framework for studying cholesterol interactions with membrane proteins to regulate protein functions and for understanding the pathogenic role of cholesterol in diseases.

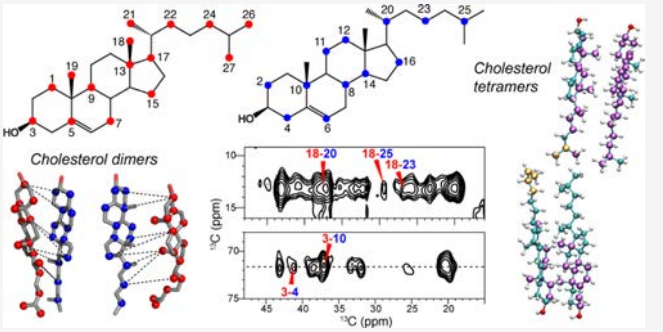

INTRODUCTION

Cholesterol, an amphiphilic sterol that makes up 20−60% of lipids in mammalian cell membranes,[1,2] has a strong influence on the physical properties of phospholipid bilayers and the structure and function of membrane proteins therein.[3−5] Cholesterol broadens the transition between the liquid-crystalline phase and gel phase of lipid bilayers and is a key constituent of the liquid-ordered (L_o) phase in binary and ternary lipid mixtures,[6−8] which underlies detergent-resistant rafts in cell membranes.[9,10] Cholesterol also regulates the oligomeric structure and function of membrane proteins such as G-protein-coupled receptors (GPCRs)[11] and viral fusion proteins.[12] Cholesterol accomplishes these functions by binding to exposed protein surfaces or internal protein cavities between transmembrane (TM) helices. Misregulation of cholesterol homeostasis is associated with many diseases such as cardiovascular diseases and Alzheimer's disease.[13]

Despite the extensive literature about the impact of cholesterol on the lipid membrane structure and dynamics, direct experimental information about the molecular structure of cholesterol assemblies remains scarce. Based on the cholesterol concentrations at which abrupt changes are detected in wide-angle X-ray diffraction data, EPR spectra, and nuclear magnetic resonance (NMR) spectra, Martin and Yeagle proposed the existence of face-to-face cholesterol dimers in lipid bilayers.[14] Recent all-atom molecular dynamics (MD) simulations supported this notion, showing that face-to-face cholesterol dimers with preferred structures exist at a range of membrane cholesterol concentrations.[15] In membrane protein crystal structures solved in the absence of phospholipids, face-to-face cholesterol dimers have been observed between TM helices.[11] However, the specificity and physiological relevance of such cholesterol dimers are usually unknown or questionable because of the use of monoolein: cholesterol mixtures for protein crystallization. A different type of cholesterol dimer, formed across two lipid leaflets in a tail-to-tail fashion, has also been proposed. This model was put forward to explain differential scanning calorimetry (DSC)

Received: November 26, 2020
Revised: January 21, 2021

data on the freezing-point depression of cholesterol-containing DPPC bilayers[16] and was later supported by fluorescence data.[17] In spite of these studies, no direct experimental data of the molecular structures of the putative cholesterol dimers and oligomers in lipid membranes are so far available.

Here, we report the first direct observation of the structures of cholesterol dimers and higher-order oligomers in phospholipid bilayers, using solid-state NMR (SSNMR) and all-atom molecular dynamics simulations. Solid-state NMR is well-suited for characterizing the dynamic structures of lipid membranes in a nonperturbing fashion.[18,19] Using metabolically ^{13}C-labeled cholesterol,[20−23] we have detected face-to-face cholesterol dimers in both palmitoylsphingomyelin (PSM)-containing membranes and low-melting phospholipid membranes. Using tail ^{13}C-labeled and tail-fluorinated cholesterol and ^{13}C and ^{19}F spin diffusion NMR, we also observed cholesterol tetramers at membrane cholesterol concentrations that mimic virus lipid envelopes and cholesterol-rich domains of cell membranes. MD simulations of 1-palmitoyl-2-oleoyl-*glycero*-3-phosphocholine (POPC)/PSM/CHOL membranes support these experimental data and give additional information about the population distribution, lifetime, and molecular packing of these nanoscopic cholesterol clusters. Based on these observations, we propose that dimers are the predominant basic structural unit of cholesterol in biological membranes and cholesterol dimers mediate protein−cholesterol and protein−protein interactions.

MATERIALS AND METHODS

Expression and Purification of ^{13}C-Enriched Cholesterol. ^{13}C-enriched cholesterol (CHOL) was produced in the *Saccharomyces cerevisiae* strain RH6829,[20,21] following previously described protocols with slight modifications.[22,23] About 20−45 mg of cholesterol was purified from each liter. 1-^{13}C CHOL was labeled using 2-^{13}C sodium acetate, whereas 2-^{13}C CHOL was labeled using 1-^{13}C sodium acetate. Note that the ^{13}C labeling level is twofold higher using sodium acetate compared to glucose as the precursor.[22]

Yeast cells were grown in YPD-rich media (1% yeast extract, 2% peptone, and 2% dextrose) for 40 h before 100 μL was used to inoculate 1 L of production media. The medium for producing ^{13}C-labeled CHOL consists of, per liter, 0.90 g ^{13}C-labeled sodium acetate (Cambridge Isotope Laboratory), 7 g yeast nitrogen base (Amresco, without amino acids, with ammonium sulfate), 40 mg Leu, 40 mg uracil, 10 mg His, 20 mg Met, 20 mg Trp, and 20 g dextrose (Fisher) added from a sterile stock solution. After incubation in a shaker for 40 h at 30 °C and 220 rpm, the yeast cells were washed with chilled 5% trichloroacetic acid and then washed with chilled water before drying. Hydrolysis of cholesteryl esters was performed in 10.5 mL of extraction cocktail per 0.5 g dry cells for 2 h at 85 °C. The cocktail consists of 1 part 60% (w/v) aqueous KOH, 1 part 0.5% (w/v) methanolic pyrogallol, and 1.5 parts methanol. The free sterols were extracted three times into 100−150 mL petroleum ether and dried under a stream of N_2 gas. The ^{13}C-labeled cholesterol was purified using reversed-phase HPLC on a Vydac C18 column (5 μm particles, 4.6 mm i.d. × 100 mm) under isocratic conditions of 30% solvent A (90% ethanol, 5% isopropanol, and 4.6% methanol) and 70% solvent B (acetonitrile) at a flow rate of 1.5 mL/min. The final purified yields were 43.6 mg for 1-^{13}C CHOL and 19.9 mg for 2-^{13}C CHOL.

Preparation of Membrane Samples. Commercial cholesterol used in this study included natural abundance cholesterol, C25-, C26-, C27-^{13}C CHOL, and 25,26,26,26,27,27,27-heptafluorocholesterol (F7-CHOL) (Sigma-Aldrich). POPC, 1-palmitoyl-2-oleoyl-*sn*-glycero-3-phospho-(1′-*rac*-glycerol) (POPG), 1-palmitoyl-2-oleoyl-*sn*-glycero-3-phosphoethanolamine (POPE), and egg sphingomyelin were purchased from Avanti Polar Lipids. Egg sphingomyelin contains 86% PSM and is thus referred to as PSM throughout the text. To investigate the generality of cholesterol clustering in eukaryotic membranes, including both cell membranes and virus lipid envelopes, we prepared three complex lipid mixtures termed VM+ membranes.[24,25] These VM+ membranes contain equimolar amounts of POPC, POPE, and PSM and 17, 20, and 44 mol % CHOL (Table S1). The phospholipid and sphingolipid ratios were chosen to be intermediate between those of cell membranes and virus envelopes,[1,26,27] whereas the two low-cholesterol samples mimic the cell membrane composition and the highest cholesterol sample mimics the influenza and HIV virus envelopes.[1,26] We also prepared two model membranes containing POPC/POPG/CHOL, with the POPC/POPG molar ratio of 4:1 and the CHOL concentration of 17 and 44 mol %.

All lipids were first dissolved in chloroform or chloroform with ∼5% methanol and mixed at the desired ratios. The organic solvents were then removed with a stream of nitrogen gas. The lipid film was redissolved in ∼300 μL of cyclohexane and lyophilized overnight. The dried membrane was rehydrated by dissolution in 3 mL buffer (20 mM Tris, pH 7.5) and then cycled seven times between liquid nitrogen and a 37 °C water bath to form multilamellar vesicles. The membrane vesicle was pelleted by ultracentrifugation at 160,000*g* and 4 °C for 4 h. After removing the supernatant, the wet pellet consisted of ∼30 mg lipid and ∼200 mg buffer. The samples were dried to ∼50% lipid (w/w) by brief lyophilization, which removes water at a rate of ∼1 mg/min. The membrane pellet was then packed into Bruker 4 mm magic-angle spinning (MAS) rotors by centrifugation at 3000*g* for 10 min. All membrane samples exhibit uniaxial ^{31}P powder line shapes (data not shown), indicating that regardless of whether CHOL is fluorinated or ^{13}C-enriched, these lipid membranes have well-ordered lamellar morphology.

Solid-State NMR Spectroscopy. Most solid-state NMR experiments were conducted on a Bruker 400 MHz AVANCE III-HD spectrometer using wide-bore 4 mm MAS probes tuned to either ^{1}H/^{19}F/^{13}C or ^{1}H/^{31}P/^{13}C frequencies. Typical radio frequency (rf) field strengths were 62−90 kHz for ^{1}H, 62−71 kHz for ^{19}F, 50 kHz for ^{31}P, and 50 kHz for ^{13}C. ^{13}C chemical shifts were externally referenced to the 38.48 ppm methylene resonance of adamantane on the TMS scale. ^{31}P chemical shifts were referenced to the hydroxyapatite signal at 2.73 ppm on the phosphoric acid scale. ^{19}F chemical shifts were referenced to the Teflon signal at −122.0 ppm on the $CFCl_3$ scale.

One-dimensional and 2D ^{19}F and ^{13}C NMR experiments were conducted at 273 K or 235−245 K at MAS frequencies of 5.0 and 5.5 kHz. The 2D ^{13}C−^{13}C correlation spectra were measured using 300 ms CORD mixing[28] for chemical shift assignments and 500−750 ms CORD mixing for measuring intermolecular correlations. The 2D ^{19}F−^{19}F correlation spectra were measured using CORD mixing times of 10−100 ms.

https://dx.doi.org/10.1021/acs.jpcb.0c10631
J. Phys. Chem. B XXXX, XXX, XXX−XXX

To investigate the cholesterol cluster size, we implemented a novel 2D CODEX experiment with ^{13}C or ^{19}F detection[29−31] (Figure 3a). In the 1D CODEX experiment, a train of rotor-synchronized 180° pulses were applied before and after a mixing period t_{mix} to recouple the chemical shift anisotropy (CSA). If the CSA tensor orientation changes during t_{mix} because of molecular motion or spin diffusion, then the intensity of the stimulated echo decreases. The intensity decay rate and the equilibrium intensity give information about the internuclear distances and oligomeric number, respectively. However, apart from this anisotropic spin exchange, the multiple ^{13}C-labeled CHOL and F7-CHOL also undergo isotropic spin exchange among the chemically inequivalent sites in each molecule. Therefore, the 1D CODEX spectra do not exclusively report intermolecular information about the oligomeric size. The 2D CODEX experiment distinguishes the isotropic and anisotropic spin exchange mechanisms by inserting a t_1 evolution period before the first CSA recoupling period. Similar to 1D CODEX, the 2D CODEX experiment was conducted in pairs: a control experiment (S_0) contains a short t_{mix} period and a long t_z period to correct for T_1 relaxation effects, whereas the exchange (S) experiment contains a long t_{mix} period and a short t_z period. The sum of the two mixing times is the same between the S_0 and S experiments. The intensity ratios, S/S_0, of the diagonal peaks of the 2D spectra exclusively result from the anisotropic spin exchange and thus report the oligomeric number.

The ^{19}F CODEX decay for type-*a* cholesterol in the 44% CHOL VM+ membrane was simulated using an exchange matrix formalism.[31] The magnetization exchange rate depends on the square of the distance-dependent $^{19}F-^{19}F$ dipolar couplings and the overlap integral $F(0)$. We used an overlap integral of 37 μs based on model compound experiments under 8 kHz MAS. Approximate intermolecular distances were taken from an MD-simulated structure of the $\alpha\alpha$ dimers.[15] We approximated each CF_3 group as a single ^{19}F spin entity with 1.5-fold times stronger dipolar couplings because of the rapid three-site exchange within each CF_3 group.[32] Thus, two cholesterol molecules possessing four CF_3 groups were represented by four spins in our simulation. We assumed a rectangular geometry with an intramolecular CF_3-CF_3 distance of 3.2 Å and an average intermolecular distance of 5 Å to simplify the calculation.

Molecular Dynamics Simulation Protocols. We simulated various VM+ lipid bilayers and POPC/PSM/CHOL bilayers with 44 and 17 mol % CHOL, mimicking experimental conditions. The POPC/PSM/CHOL bilayers (4:4:2 M ratios) were simulated both from a phase-separated state and from a miscible state, the former stabilized by a 2:1 x/y aspect ratio to overcome the instability because of finite size effects.[33] A POPC/PSM/CHOL bilayer at 3:3:4 M ratio was also simulated. All simulations were performed using the GROMACS 2018.3 package,[34] employing the CHARMM36 force field for lipids.[35] These all-atom simulations were conducted in an aqueous environment (22.5 Å water thickness from each side of the membrane) defined by the TIP3P water model[36] with a physiological salt concentration of 150 mM NaCl. Initial systems were constructed and equilibrated using the CHARMM-GUI protocols.[37−39] Production simulations were carried out under constant NPT conditions with a time step of 2 fs using a parallelized linear constraint solver to constrain the H-bond lengths.[40] The temperature was kept constant using the Nosé-Hoover thermostat[41,42] with a 1 ps coupling constant, and pressure was controlled by a Parrinello-Rahman barostat[43] with a semi-isotropic coupling scheme and a coupling constant of 5 ps at 1 bar pressure. The smooth particle-mesh Ewald method was used to model long-range interactions with a grid spacing of 0.12 nm and a 1.2 nm cutoff.[44] Van der Waals interactions were truncated using a force switch function from 1.0 to 1.2 nm. Structures were rendered using VMD.[45] The analyses were conducted with in-house python scripts utilizing NumPy, SciPy, and MDAnalysis[46,47] libraries.

VM+ bilayers were composed of 1000 randomly placed lipids. Three systems at 17 mol % CHOL and two systems at 44 mol % CHOL were simulated for 1 μs each at 273 K and were quenched to 243 K and simulated for an additional 1 μs. Miscible POPC/PSM/CHOL bilayers were composed of 400 randomly placed lipids. Two 1 μs trajectories and one 2 μs trajectory for both 4:4:2 and 3:3:4 bilayers were simulated at 295 K. Four 500 ns simulations initiated from the last conformation of the 4:4:2 bilayer and the 3:3:4 bilayer simulations at 243 and 273 K, respectively, were performed. Phase-separated POPC/PSM/CHOL 4:4:2 bilayers were composed of 800 lipids, placed into a stripe-shaped phase separation system with a 2:1 x/y aspect ratio to stabilize the phase-separated state.[33] Cholesterols were distributed in a 2:1 ratio between the POPC and PSM phases, consistent with the observations in experiment and simulation.[48−50] This system was simulated for 1 μs at 295 K, and the final configuration of this system was used to initiate a 500 ns simulation at 273 K.

To examine the effects of fluorination on CHOL, 25,26,26,26,27,27,27-heptafluorocholesterol (F7-CHOL) parameters were generated by combining the CGenFF 4.1 parameters[51−55] for the F7-CHOL tail and CHARMM36 parameters of the sterol ring.[56] We note that these parameters were not further optimized, and all charge assignments and internal parameters with nonzero penalty scores for the F7-CHOL tail are noted in Tables S2−S5. Equilibrated membrane configurations from the miscible state POPC/PSM/CHOL 4:4:2 simulations were then extracted; CHOL structures were substituted with F7-CHOL structures, energy-minimized, equilibrated, and simulated up to 500 ns with the new F7-CHOL parameters at 295 K.

Structural Analysis Methods for Simulated Cholesterol Clusters. *CHOL−CHOL Crick Angles.* To characterize the CHOL−CHOL dimer ensemble, we employed two angles defining the relative orientations of a CHOL−CHOL pair, which we refer to as "Crick angles", Ψ_1 and Ψ_2.[15] This requires defining an axis between two CHOL molecules that are in contact, and the vectors of the CHOL methyl group (C19), defining the orientation of each CHOL β face. For a dimer with components *i* and *j*, Crick angles were defined in terms of $C19(i) - COM(i) - COM(j)$ (Ψ_1) and $C19(j) - COM(j) - COM(i)$ (Ψ_2). CHOL is considered to be in contact if the distance between the centers of mass of each sterol ring B (COM) is less than 8 Å. The closest of CHOL satisfying this COM pair distance criterion to the *i*th CHOL, if any, is regarded as the *j*th CHOL in the dimer.

CHOL−CHOL Contacts Maps, Residence Times, and Cluster Distributions. We evaluated the CHOL−CHOL contact distribution of intraleaflet, interleaflet, and all (without discrimination between the intra- and interleaflets) forms of CHOL contacts *via* heavy-atom contacts within a 5 Å distance cutoff. The residence times for CHOL dimers are calculated from the instance of initiating any heavy atom contact between

https://dx.doi.org/10.1021/acs.jpcb.0c10631
J. Phys. Chem. B XXXX, XXX, XXX−XXX

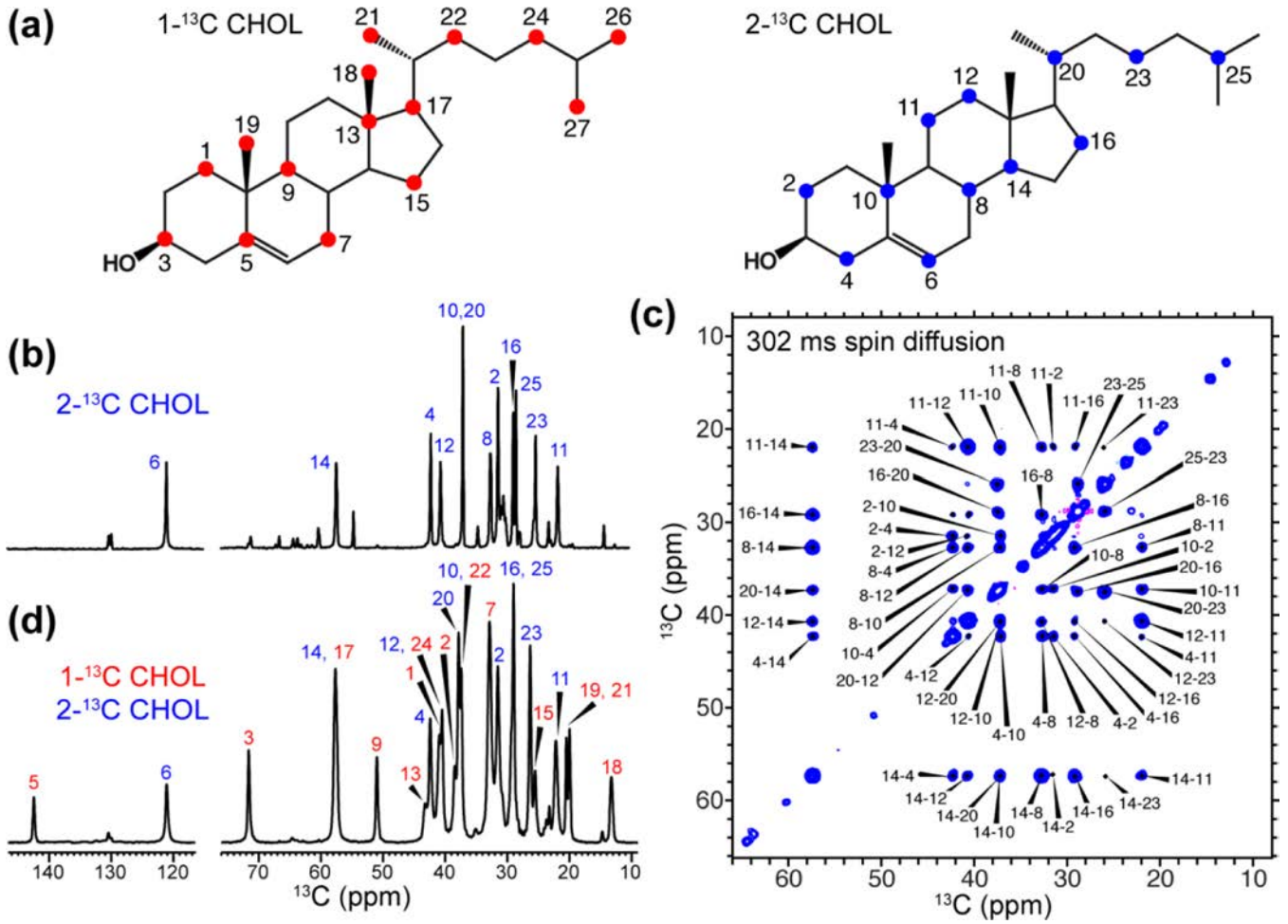

Figure 1. Yeast ^{13}C-labeled cholesterol and ^{13}C chemical shift assignment. (a) Cholesterol structure and ^{13}C-labeled sites in 1-^{13}C CHOL and 2-^{13}C CHOL. (b) ^{13}C direct polarization spectrum of 2-^{13}C CHOL in POPC/POPG bilayers at 273 K. (c) 2D ^{13}C−^{13}C correlation spectrum of 2-^{13}C CHOL in POPC/POPG bilayers at 273 K, measured with a mixing time of 302 ms. (d) ^{13}C CP spectrum of 1-^{13}C and 2-^{13}C CHOL (1:1) mixed VM+ membranes. Red and blue assignments indicate 1-^{13}C and 2-^{13}C CHOL peaks, respectively.

the CHOL pair, checking that this condition is met at 100 ps intervals until no contact between the pair is detected. We have also extended the heavy-atom contact analysis to estimate the CHOL−CHOL oligomer size probability distribution of intraleaflet, interleaflet, and all CHOL−CHOL pairs.

Z-Axial Position Distributions. The z-axial probability density of CHOL tail atoms was used to provide a perceptible representation of interleaflet interactions. This is computed by centering the z-axial positions of selected molecular groups about the bilayer midplane and 2 Å width bins.

Displacement Pair Correlation Function. The average displacement pair correlation function H for various displacements in time $t - t_0$ for the motion of the ith and jth cholesterol of N_{dimers}-dimerized CHOLs present at each of M initial times denoted by $t_{0,k}$ is calculated in a manner similar to the method of Ando and Skolnick.[57]

$$\langle H(t-t_0)\rangle = \frac{1}{M}\sum_{k}^{M} \frac{\sum_{i,j}^{N_{dimers}} \Delta\vec{r}_i(t-t_{0,k})\cdot\Delta\vec{r}_j(t-t_{0,k})}{\sqrt{\sum_{i}^{N_{dimers}} |\Delta\vec{r}_i(t-t_{0,k})|^2}\sqrt{\sum_{j}^{N_{dimers}} |\Delta\vec{r}_i(t-t_{0,k})|^2}}$$

where $\Delta r_i \rightarrow (t - t_{0,k})$ is the displacement vector of CHOL i at time t from its position at time $t_{0,k}$.

RESULTS

Cholesterol Forms Face-to-Face Dimers at a Range of Concentrations in Lipid Membranes. To investigate whether cholesterol self-associates in lipid membranes, we produced two complementary ^{13}C-labeled CHOL samples using the mutant yeast *S. cerevisiae* RH6829.[20,21] This genetically engineered yeast strain contains enzymes for the biosynthesis of cholesterol instead of ergosterol and allows a high-yield production (~30 mg) of^{13}C-labeled CHOL per liter of culture. We used sodium acetate as the carbon precursor, which gives twice the ^{13}C-labeling level of glucose.[22] The 2-^{13}C-labeled sodium acetate enriches 15 carbons in cholesterol, including the hydroxy C3 and all methyl carbons (Figure 1a). We denote this compound as 1-^{13}C CHOL because the labeling pattern is identical to that produced by 1-^{13}C glucose. Complementarily, 1-^{13}C sodium acetate enriches the other 12 carbons, most of which lie on the sterol rings. We denote this compound as 2-^{13}C CHOL.

One- and two-dimensional ^{13}C NMR spectra (Figure 1b,c) of 2-^{13}C CHOL in POPC/POPG membranes show resolved ^{13}C chemical shifts, which are readily assigned based on the peak connectivity pattern (Table S6). The ^{13}C linewidths are ~0.2 ppm at 273 K, similar to those of 1-^{13}C CHOL.[23] Most ^{13}C chemical shifts of the sterol rings resonate between 20 and

https://dx.doi.org/10.1021/acs.jpcb.0c10631
J. Phys. Chem. B XXXX, XXX, XXX−XXX

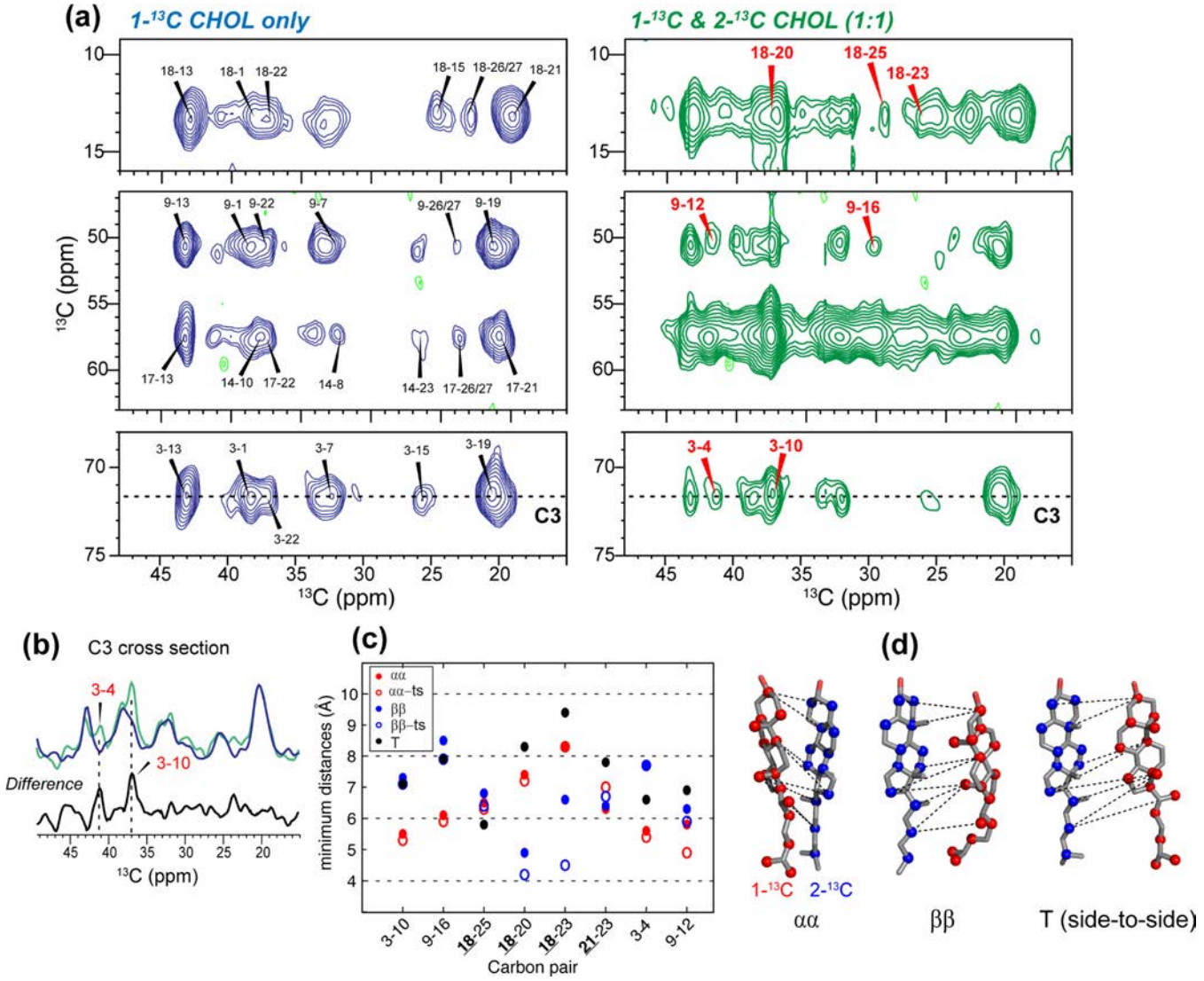

Figure 2. Two-dimensional $^{13}C-^{13}C$ correlation spectra revealing cholesterol self-association in lipid membranes. (a) 2D spectra of the 44% CHOL VM+ membrane, measured at 240 K using a ^{13}C spin diffusion mixing time of 750 ms. Comparison of the 1-^{13}C CHOL spectrum (blue) with the 1-^{13}C and 2-^{13}C CHOL (1:1) spectrum (green) reveals intermolecular correlation peaks (assigned in red) in addition to intramolecular correlations (assigned in black). (b) C3 cross section (71 ppm) from the two 2D spectra. The difference between the 1-^{13}C CHOL sample and the mixed 1-^{13}C and 2-^{13}C CHOL sample confirms the assignment of the intermolecular C3−C10 and C3−C4 cross peaks. (c) Shortest intermolecular distances in MD-simulated cholesterol dimers for the observed intermolecular $^{13}C-^{13}C$ correlation peaks. The $\alpha\alpha$ and $\beta\beta$ dimers exhibit relatively short intermolecular distances, whereas the T dimer shows longer distances. Bold and underlined carbons are the methyl groups. (d) SSNMR-detected $^{13}C-^{13}C$ contacts superimposed onto the representative models of intraleaflet $\alpha\alpha$, $\beta\beta$, and T dimers.[15] These structural models are refined in Figure 5.

60 ppm, which is a smaller range than the ^{13}C chemical shift dispersion of 1-^{13}C CHOL. Nevertheless, the peaks are sufficiently resolved to allow the full assignment of the ^{13}C spectra of a 1:1 mixture of 1-^{13}C and 2-^{13}C CHOL (Figures 1d, S1).

We investigated cholesterol clustering in a virus-mimetic membrane (VM+) containing POPC, POPE, PSM, and CHOL and a POPC/POPG/CHOL membrane. The CHOL molar concentrations in these membranes range from 17 to 44%, which correspond to the mass concentrations of 10−28 wt %. Most NMR experiments were conducted at moderately low temperatures of 240−273 K. This low temperature is necessary to slow down the translational and rotational diffusion of CHOL, which would average the dipolar couplings needed to detect intermolecular contacts. MD simulations confirm that CHOL self-assembly is observed over the range of membrane compositions and temperatures studied (*vide infra*).

To investigate intermolecular CHOL−CHOL contacts, we measured the 2D $^{13}C-^{13}C$ correlation spectra of membranes containing an equimolar mixture of 1-^{13}C and 2-^{13}C CHOL. We first examined the 44% CHOL VM+ membrane and used long spin diffusion mixing times of 500−750 ms to measure long-range correlation peaks. At 273 K, most cross peaks are intramolecular, within 1-^{13}C CHOL or within 2-^{13}C CHOL. The only intermolecular correlation peak is observed between the hydroxyl C3 of 1-^{13}C CHOL and C10 of 2-^{13}C CHOL (Figure S1). To restrict the translational diffusion of cholesterol, we decreased the temperature to 240 K. This caused moderate line broadening, but the spectra still retained a number of resolved peaks. These include the 12.8 ppm C18

https://dx.doi.org/10.1021/acs.jpcb.0c10631
J. Phys. Chem. B XXXX, XXX, XXX−XXX

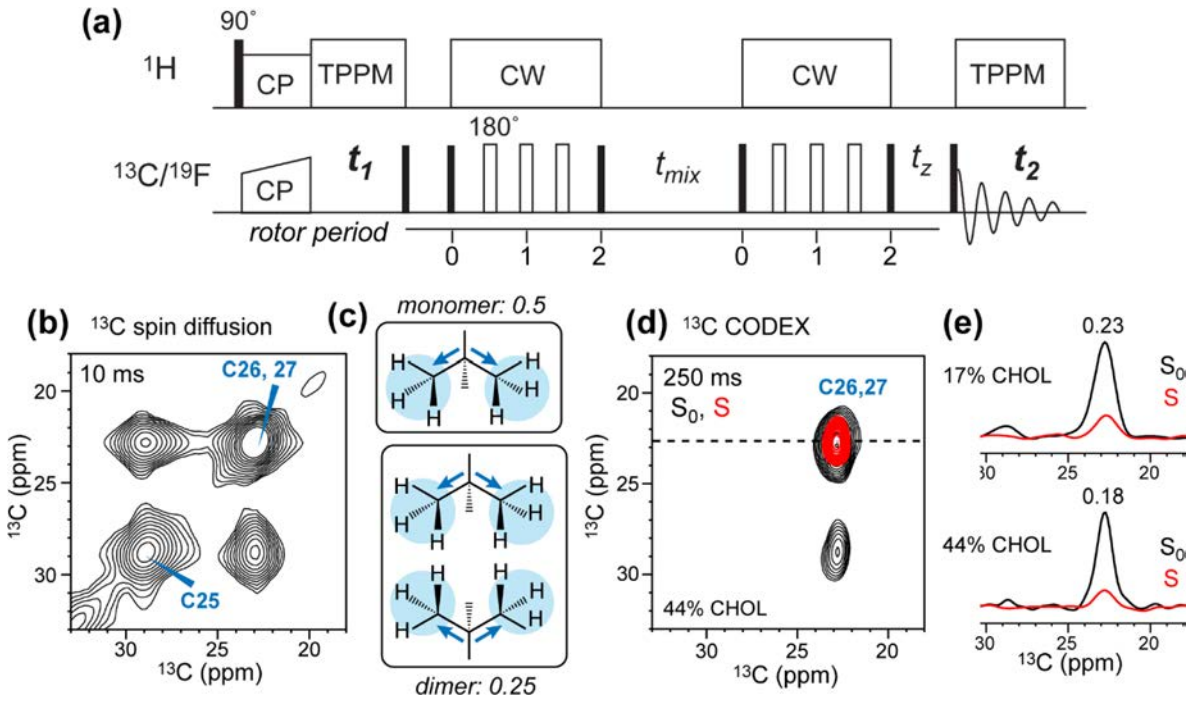

Figure 3. ^{13}C CODEX experiments indicating cholesterol dimer formation in lipid membranes. (a) Pulse sequence of the 2D CODEX experiment. The X-channel (^{13}C or ^{19}F) t_1 evolution period allows chemical shift encoding, which distinguishes isotropic spin exchange from anisotropic spin exchange. (b) 2D ^{13}C−^{13}C CORD spin diffusion spectrum of C25-, C26-, C27-^{13}C CHOL in the 44% VM+ membrane. Intramolecular C25 to C26/C27 cross peaks are observed, as expected. (c) Predicted CODEX equilibrium S/S_0 values for CHOL monomers and dimers. Each CHOL contains two methyl groups (C26 and C27), whose ^{13}C chemical shift tensor orientations differ. Thus, a CHOL monomer causes an equilibrium S/S_0 value of 0.5, whereas a CHOL dimer with four methyl groups will cause an equilibrium S/S_0 value of 0.25. (d) 2D ^{13}C CODEX S_0 (black) and S (red) spectra of C25-, C26-, and C27-^{13}C labeled CHOL in the 44% VM+ membrane. Intensity dephasing of the diagonal C26/C27 peak is observed. (e) 1D cross sections of the 2D ^{13}C CODEX spectra for the 17 and 44% VM+ membranes. The C26/C27 diagonal peak decays to 0.23 in the 17% CHOL membrane, indicating an average oligomer size of dimers. At a CHOL concentration of 44%, the diagonal peak decays to 0.18, indicating a distribution of oligomer sizes that includes larger species than dimers.

peak, the 50.9 ppm C9 peak, and the 71.4 ppm C3 peak, which serve as markers for intermolecular correlations. In total, we assigned 10 intermolecular correlations between 1-^{13}C and 2-^{13}C CHOL, such as C18−C23, C9−C16, C3−C4, and C3−C10 (Figure 2a,b, Table S7). Comparison with the 1-^{13}C CHOL-only spectra validates the intermolecular origin of these cross peaks. Reducing the CHOL concentration to 20 mol % in the VM+ membrane did not remove the intermolecular cross peaks (Figure S2), indicating that the observed self-association is an intrinsic property of CHOL.

Recent MD simulations suggested that cholesterol can dimerize into several structures, depending on whether the smooth face (α) or the methyl-rich rough face (β) lies at the dimer interface. These dimers include $\alpha\alpha$, $\beta\beta$, and side-to-side (T) dimers, with characteristic stabilities and populations.[15] At room temperature, these dimers further adjust their conformations through twisting (t) and sliding (s) of the associated molecules. To investigate which MD-simulated dimer structures agree best with the experimentally measured intermolecular ^{13}C−^{13}C correlations, we analyzed the intermolecular distances in the simulated dimers (Figure 2c). $\alpha\alpha$ and $\alpha\alpha$-ts dimers exhibit short intermolecular distances between nonmethyl carbons, whereas $\beta\beta$ and $\beta\beta$-ts dimers exhibit short distances between methyl carbons such as C18 and C21 in one molecule and nonmethyl sterol carbons in the other molecule. Thus, the fact that both nonmethyl and methyl correlation peaks are observed in the 2D spectra is consistent with the presence of both $\alpha\alpha$ and $\beta\beta$ classes of dimers. In contrast, intermolecular distances for the simulated side-to-side T dimer are much longer; thus, they are the least consistent with the ^{13}C−^{13}C cross peaks. As ^{13}C spin diffusion NMR is sensitive to distances less than ∼8 Å, the ^{13}C−^{13}C correlations support the existence of the face-to-face $\alpha\alpha$ and $\beta\beta$ dimers but not the side-to-side T dimers in the 44% CHOL membrane.

Cholesterol Self-Associates as Dimers and Tetramers at Different Membrane Concentrations. Although the 2D ^{13}C−^{13}C correlation spectra provide evidence for the existence of face-to-face dimers, they do not indicate whether tail-to-tail dimers are present, nor whether larger cholesterol oligomers exist. To address these questions, we turned to the CODEX experiment, using both ^{13}C-labeled CHOL and fluorinated CHOL. The CODEX technique, originally developed as a 1D experiment,[29] detects the relaxation-corrected intensity (S/S_0) of a stimulated echo to report the number of spins in close proximity. These spins have the same isotropic chemical shift but different anisotropic shifts because of different molecular orientations.[30,31] When the magnetization is transferred and equilibrated among these spins, a cluster with an oligomeric number of M should give an equilibrium CODEX intensity of 1/M. However, the 1D CODEX experiment cannot be directly applied to the methyl ^{13}C-labeled CHOL because an isotropic spin exchange between the CH group (C25) and the two methyl carbons (C26 and C27) within each molecule occurs to reduce the echo intensity. Similarly, isotropic ^{19}F spin exchange will also occur between the CF_3 groups and the CF group in F7-CHOL, decreasing the 1D ^{19}F CODEX intensities. To

https://dx.doi.org/10.1021/acs.jpcb.0c10631
J. Phys. Chem. B XXXX, XXX, XXX−XXX

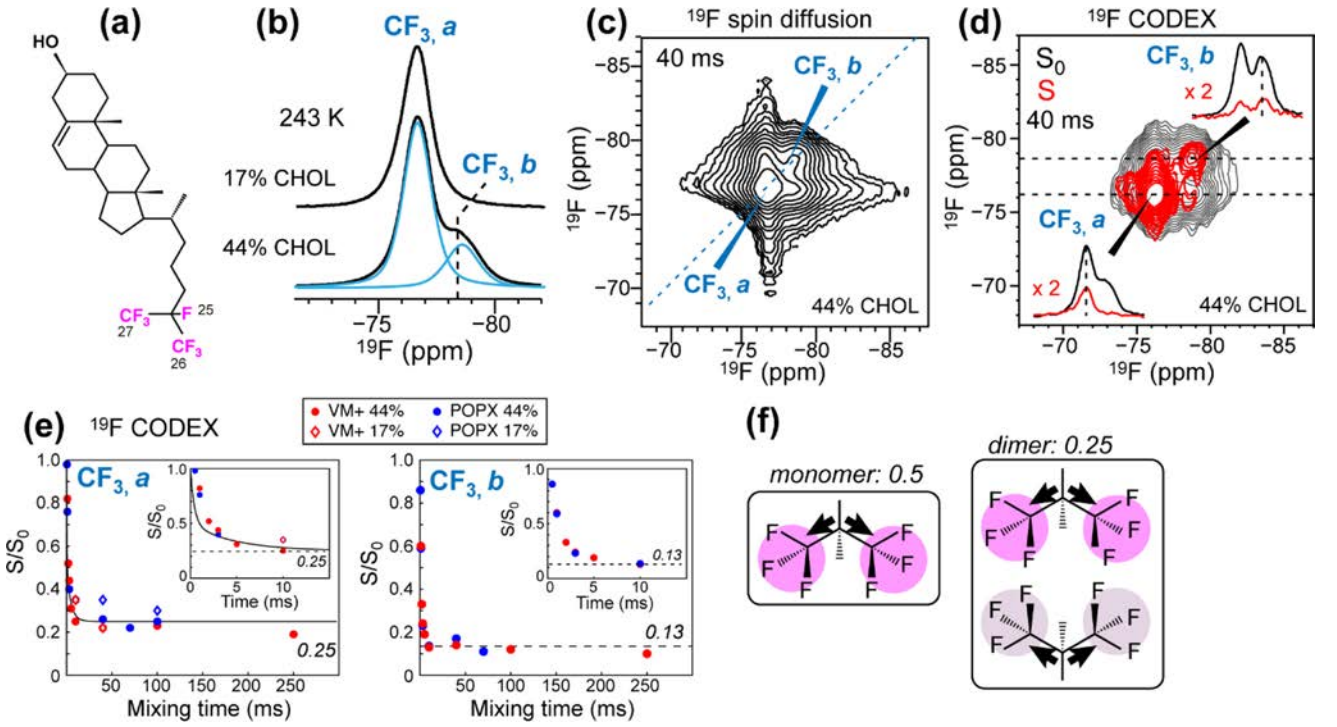

Figure 4. ^{19}F NMR evidence for cholesterol oligomerization in lipid membranes. (a) Structure of F7-CHOL. (b) ^{19}F NMR spectra of F7-CHOL in VM+ membranes containing 17 and 44% CHOL. The spectra were measured at 243 K. At the high CHOL concentration, a second ^{19}F peak, termed type-*b*, is observed together with the dominant type-*a* signal. (c) 2D ^{19}F−^{19}F CORD spin diffusion spectrum of the 44% CHOL VM+ membrane. With 40 ms of mixing, cross peaks between type-*a* and type-*b* CF_3 signals are observed, indicating that these two conformers are close in space. (d) 2D ^{19}F CODEX S_0 and S spectra of the 44% CHOL VM+ membrane, measured at 235 K using a t_{mix} of 40 ms. (e) ^{19}F CODEX decay curves for type-*a* and type-*b* CHOL in VM+ and POPC/POPG membranes. The type-*a* peak decays to ∼0.25, whereas the type-*b* signal decays to ∼0.13. Insets show the initial regime of the decay curves. (f) Schematic of the CF_3 equilibrium S/S_0 values for CHOL monomers and dimers.

distinguish anisotropic from isotropic spin exchange, we thus extended the 1D CODEX experiment to 2D, where the diagonal peaks are unaffected by the isotropic spin exchange (Figure 3a). By measuring the 2D CODEX control (S_0) and dephased (S) spectra and analyzing the diagonal peak intensity ratio, we obtain a purely anisotropic spin exchange that reflects the oligomeric number of cholesterol.

Figure 3b shows the 2D ^{13}C−^{13}C spin diffusion spectrum of C25-, C26-, and C27-^{13}C CHOL in the 44% CHOL VM+ membrane. The C25 peak at 29 ppm is well resolved from the overlapped peak of C26 and C27 at 23 ppm. With 10 ms mixing, intramolecular cross peaks between C25 and the C26/C27 peak are already observed. We next employed the 2D ^{13}C CODEX experiment to measure the oligomeric number of cholesterol clusters. If cholesterol is exclusively monomeric, then the different orientations of the C26 and C27 ^{13}C chemical shift tensors within each molecule should cause CODEX dephasing (S/S_0) to 0.5 for the diagonal C26/C27 peak (Figure 3c). However, if cholesterol forms dimers, then the CODEX dephasing of the diagonal C26/C27 peak should decrease to 0.25 when the ^{13}C magnetization is fully equilibrated among four methyl carbons. Likewise, tetrameric cholesterol clusters should manifest an equilibrium intensity ratio of 0.125. Figure 3d shows the 2D ^{13}C−^{13}C CODEX spectrum of the 44% CHOL VM+ membrane. The spectrum was measured using a ^{13}C CSA recoupling time of 3.4 ms and a ^{13}C−^{13}C mixing time of 250 ms. For the 17% CHOL membrane, we measured an intensity ratio of 0.23, indicating that the *average* oligomer size is centered at the dimer (Figure 3e). When the CHOL concentration increased to 44%, we detected an equilibrium S/S_0 intensity ratio of 0.18. This value is much lower than the value of 0.25 expected for dimers and is consistent with the coexistence of dimers and tetramers in the membrane. Thus, these ^{13}C CODEX data indicate that cholesterol self-associates in the membrane, with an average cluster size of dimers at a membrane concentration of 17%. At a higher membrane concentration of 44%, which is typical for virus lipid envelopes, there is a significant amount of higher-order oligomers, possibly tetramers.

The isooctyl-fluorinated F7-CHOL (Figure 4a) confirms the dimerization and higher-order oligomerization of cholesterol in the membrane. F7-CHOL has pressure−area isotherms nearly identical to that of hydrogenated cholesterol, indicating that its molecular orientation and phospholipid interactions are indistinguishable from those of hydrogenated cholesterol.[58] For VM+ and POPC/POPG membranes containing 17% CHOL, ^{19}F NMR spectra show a single CF_3 peak at −76 ppm and a single CF peak at −183 ppm at low temperatures (235−243 K) (Figures 4b, S3). However, as the CHOL concentration increased to 44%, a second set of weak peaks appears, whose chemical shifts are 1.4−2.1 ppm upfield from the chemical shifts of the major species. We denote the major species as type-*a* and the minor species as type-*b*. With 44% CHOL in the membrane, the relative populations of these two species are 71 and 29%, respectively, based on spectral deconvolution. The 2D ^{19}F−^{19}F correlation spectra exhibit not only intramolecular CF_3−CF cross peaks for each cholesterol (Figure 4c) but also intermolecular cross peaks between type-*a* and type-*b* CF_3 signals (Figure S3c), indicating that the

https://dx.doi.org/10.1021/acs.jpcb.0c10631
J. Phys. Chem. B XXXX, XXX, XXX−XXX

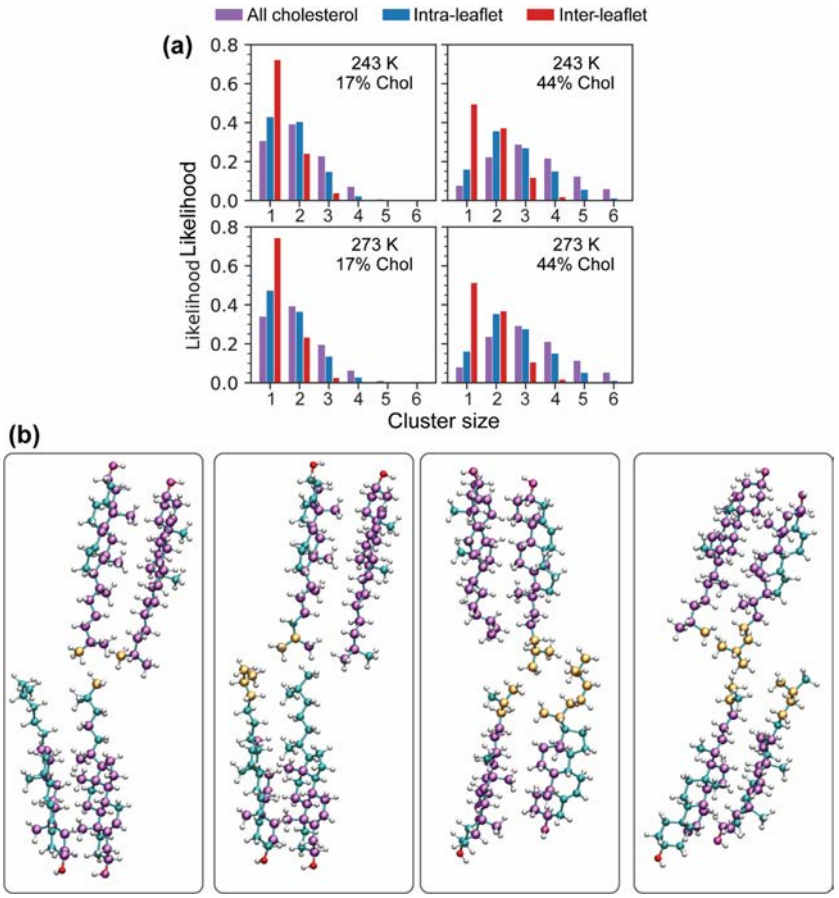

Figure 5. Simulated intraleaflet, interleaflet, and all forms of CHOL clusters in POPC/PSM/CHOL membranes. (a) Size distributions of cholesterol clusters at 243 and 273 K. (b) Structures of the CHOL tetramers extracted from simulation trajectories. Heavy atoms within 5 Å of another CHOL's heavy atoms in the same leaflet are highlighted in purple. Heavy atoms within 5 Å of any other CHOL in the opposing leaflet are highlighted in orange.

isooctyl tails of the two types of cholesterol are in close proximity with each other.

The 2D $^{19}F-^{19}F$ CODEX S_0 and S spectra of the 44% CHOL VM+ membrane show the same trend as the 2D ^{13}C CODEX spectra. With a CODEX mixing time of 40 ms, the type-*a* CF_3 diagonal peak decayed to ∼0.25, whereas the type-*b* CF_3 diagonal peak decayed to ∼0.13 (Figure 4d). By 100 ms, the CODEX S/S_0 values equilibrated to 0.23 and 0.12, respectively (Figure 4e). The fluorine atoms in each CF_3 group are equivalent because of the fast methyl three-site jumps. The motionally averaged ^{19}F chemical shift tensors of C26 and C27 are thus oriented at 109° from each other. Therefore, just like 2D ^{13}C CODEX, a cholesterol monomer should exhibit an equilibrium S/S_0 value of 0.5 for the CF_3 signal, a cholesterol dimer should exhibit a value of 0.25, whereas a cholesterol tetramer should exhibit a value of 0.125 (Figure 4f). Thus, the measured S/S_0 value of ∼0.23 indicates that type-*a* cholesterol has an average oligomer size of dimers, whereas the S/S_0 value of ∼0.12 for type-*b* cholesterol indicates that these cholesterol species are on average tetrameric. These oligomer sizes are average values, as a single equilibrium intensity cannot report the oligomer size distribution. Odd-numbered clusters such as trimers cannot be excluded. Indeed, MD simulations indicate the presence of trimers in addition to dimers and tetramers (*vide infra*).

The POPC/POPG membranes with 17 and 44% CHOL show the same CODEX intensities as the VM+ membranes (Figure 4e), indicating that CHOL tetramerization is not unique to the PSM-containing membranes. At a longer mixing time of 250 ms, the CODEX intensities in the VM+ membrane decayed slightly further, to 0.19 for the type-*a* CF_3 peak and 0.10 for the type-*b* CF_3 peak, suggesting that multiple dimers and tetramers may lie in close proximity.

Molecular Dynamics Simulations of Cholesterol Clusters. To corroborate the solid-state NMR data and to investigate the lifetimes, spatial distribution, and molecular structures of cholesterol clusters in lipid membranes, we conducted all-atom simulations of VM+ membranes containing 44 and 17 mol % cholesterol and POPC/PSM/CHOL membranes of varying composition and miscibility. The simulated membranes were modeled using the CHARMM36 force field for lipids.[35] Each lipid bilayer was immersed in a TIP3P water layer[36] containing a physiological salt concentration of 150 mM NaCl.

We observed both intraleaflet and interleaflet cholesterol−cholesterol dimers and higher-order oligomers (Figure 5), in good agreement with the NMR data. The minimum unit of dimers shows *αα*, *αα*-ts, *ββ*, *ββ*-ts, and T conformations (Figures S4, S5), which were previously predicted in the simulations of membranes with 10 and 20% CHOL.[15] The presence of *αα*, *αα*-ts, *ββ*, and *ββ*-ts states is consistent with that of the 2D $^{13}C-^{13}C$ correlation spectra (Figure 2c). These four dimer structures are relatively stable, whereas the T-

https://dx.doi.org/10.1021/acs.jpcb.0c10631
J. Phys. Chem. B XXXX, XXX, XXX−XXX

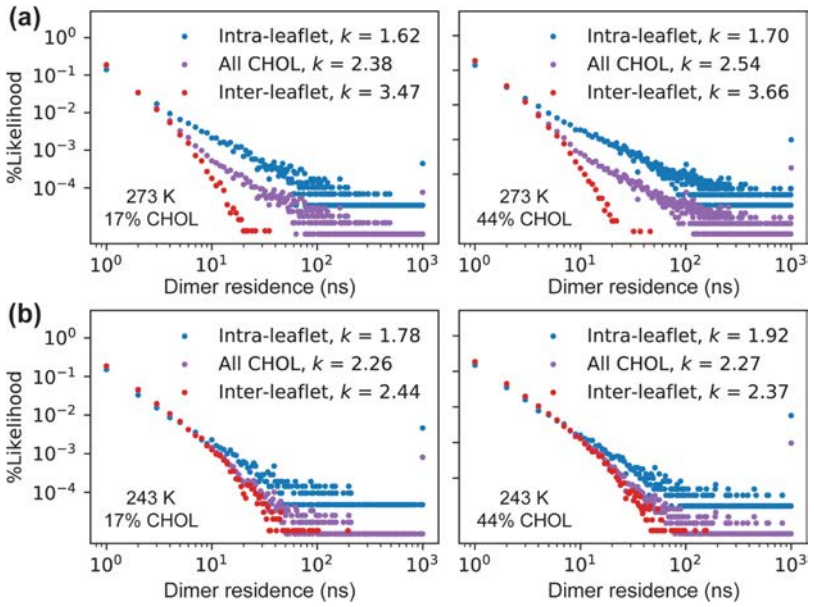

Figure 6. Residence time distributions of CHOL−CHOL dimers in VM+ membranes. Power law exponents describing log−log slope up to 200 ns; $\log(p) = k \log(time)$ shown in legend. (a) 273 K simulations. (b) 243 K simulations.

dimers are less stable, with residence times of less than 1 ns (Figure S6).

Though the average dimer residence lifetime is on the order of 1 ns (Table S8), dimer lifetimes of intraleaflet, interleaflet, and both intra- and interleaflet interactions follow a power law distribution. In VM+ membranes, we observe a substantial enhancement of interleaflet cholesterol interaction lifetimes when the temperature is decreased from 273 to 243 K (Figure 6). Of these, there are exceptionally long-lived dimers comprising 0.1 to 1% of all observed CHOL dimers. These long-lived dimers are observed at all temperatures, including 295 K (Figure S7a). They exhibit highly correlated motion, decaying slowly relative to the bulk of cholesterol[57] (Figure S7b). Taken together, these observations suggest that both short- and long-lived CHOL clusters exist in the VM+ and POPC/PSM membranes at CHOL concentrations of 17−44% and temperatures from 240 to 295 K.

The combination of intraleaflet and interleaflet interactions results in not only even-numbered CHOL oligomers such as dimers and tetramers but also odd-numbered oligomers such as trimers and a small percentage of pentamers (Figure 5a). Tetramers result from intraleaflet dimers contacting another dimer in the opposing leaflet (Figure 5b). Similarly, trimers result from intraleaflet dimers contacting a monomer in the opposing leaflet. We also investigated the effects of chain fluorination on CHOL−CHOL interactions. We did not observe a significant perturbation to the *z*-axial position distributions of CHOL tails or interleaflet CHOL−CHOL contacts (Figure S8). Importantly, simulations including fluorinated cholesterol analogues suggest that dimer lifetimes and cluster distributions are unaffected by chain fluorination (Figure S9).

DISCUSSION

Cholesterol Self-Associates as Dimers and Tetramers in a Variety of Phospholipid Bilayers. The ^{13}C and ^{19}F NMR spectra obtained here provide the first experimental structural evidence that cholesterol forms intra-leaflet face-to-face dimers at a membrane concentration as low as 17 mol % and forms tetramers at higher concentrations. The 17 mol% concentration corresponds to only ∼10 wt % CHOL; thus, dimerization is not because of nonspecific interactions but reflects the intrinsic propensity of CHOL to self-associate. The high CHOL concentration of 44 mol % is characteristic of the virus lipid envelopes[1,26] and liquid-ordered domains of cell membranes and is thus biologically relevant. We detected CHOL self-association in lipid membranes both with and without PSM, and both with and without POPE. Thus, this self-association is independent of liquid-disordered (L_d) phase, L_o phase, and $L_d - L_o$ phase separation. MD simulations support these experimental results, showing CHOL clustering after starting with a random distribution of CHOL in the membrane and exhibiting separation of timescales in CHOL−CHOL dimer residence times.

Previous DSC and fluorescence experiments[16,17] suggested the presence of tail-to-tail cholesterol dimers but were unable to confirm the existence of face-to-face dimers because the 7-nitrobenz-2-oxa-1,3,-diazol-4-yl (NBD) fluorescent probe in these studies was restricted to the isooctyl tail. Neutron scattering data of DPPC membranes containing 32% CHOL detected a peak that was assigned to dimeric cholesterol, separated by an average distance of 4.6 Å.[59] However, the data could not give information about the dimer structure. The ^{13}C and ^{19}F SSNMR experiments shown here circumvent these limitations by detecting the intermolecular contacts between the sterol rings as well as intermolecular contacts between the isooctyl chains, thus unambiguously proving the existence of intraleaflet face-to-face dimers.

At high membrane cholesterol concentrations, both the ^{19}F chemical shift spectra and ^{13}C and ^{19}F CODEX spin-counting data indicate that a small population (∼30%) of tetramers exists. The lowest equilibrium CODEX intensity ratio we measured was ∼0.12, consistent with the tetrameric cholesterol clusters. In principle, CODEX intensity ratios can result from a distribution of oligomer sizes. Thus, intensity ratios of 0.25 and 0.125 could result from the distributions centered on the dimer and tetramer. Indeed, MD simulations predict a distribution of both even-numbered and odd-numbered oligomers (Figures 5,

https://dx.doi.org/10.1021/acs.jpcb.0c10631
J. Phys. Chem. B XXXX, XXX, XXX−XXX

S9). On the other hand, the measured type-*a* and type-*b* CF_3 peaks have similar narrow linewidths of 1.4 and 1.8 ppm (Figure S3), implying that the oligomer size distributions are relatively narrow. Moreover, if the 17% membrane mainly consists of monomeric and trimeric cholesterol, then it is difficult to rationalize how these odd-numbered clusters would grow to an average cluster size of 4 in the 44% CHOL membrane. Because cholesterol has an approximately planar geometry, formation of even-numbered clusters is physically reasonable. MD simulations confirm that dimers and tetramers have substantial populations at high CHOL concentrations (Figure 5a).

Because C25, C26, C27-^{13}C CHOL, and F7-CHOL detect the isooctyl chain, the CODEX-reported cholesterol tetramers could result from either intraleaflet or interleaflet association of two dimers. MD simulations show that the population of tetramers is higher for two dimers that associate in a face-to-face fashion within each leaflet (Figure 5b) than for tetramers that are formed in a tail-to-tail fashion across two leaflets. Simulations also show that at 40% CHOL concentration, cholesterol can further associate into larger assemblies through cooperative interleaflet and intraleaflet contacts (Figure S9). However, the length scale of these larger aggregates is outside the range detectable by NMR.

Previous MD studies have also given insights into the spatial distribution of cholesterol in membranes across the full (0−66 mol %) range of soluble CHOL concentrations[63] and in mixtures with saturated and unsaturated lipids.[64] MD studies at higher temperatures found that cholesterol−cholesterol interactions are less stable than cholesterol−lipid interactions because the lipid ester−water hydrogen-bonding outcompetes the hydrogen bonding of the cholesterol alcohol group with water.[60−62] This defines the umbrella model, which posits that cholesterol, with its small polar head, seeks interaction with large-headgroup lipids such as phosphocholine in order to shield the bulky hydrophobic sterol body. It has been observed that monomeric cholesterol is a key contributing factor to lipid condensation and formation of the L_o phase.[65] At a moderate CHOL concentration, the L_o phase can feature CHOL in regularly spaced lattices inside of hexagonally packed lipid domains, as well as in the interstitial regions between hexagonally packed domains in which cholesterol can form higher-order aggregates.[64,66−68] Our results suggest that long-lived $\alpha\alpha$ and $\alpha\alpha$-ts CHOL dimers are found in all of these environments. At concentrations higher than 50 mol %, cholesterol "threads", the maze-like arrangements of CHOL with each molecule having only two nearest neighbors, have been suggested to form[48,66,69] Such threads seem likely to be stabilized by repeats of $\alpha\beta$ and $\alpha\beta$-ts motifs.

Significance of Cholesterol Clustering for Membrane Protein Function. How do these cholesterol dimers and tetramers impact membrane protein structure and function? We hypothesize that the face-to-face dimers may associate with membrane proteins through their methyl-studded β face, stabilized by van der Waals and CH-π interactions. An analysis of 35 structures of CHOL-bound TM domains of 22 membrane proteins (Table S9) showed that approximately two-thirds of cholesterol molecules interact with proteins through the β face.[70,71] Another analysis of 46 crystal structures of 10 GPCRs[72] found that the average protein−CHOL distances are the shortest for those involving methyl C18 and C19 atoms. These data support the notion that the cholesterol β face interacts with proteins more readily, whereas the smooth α face mediates CHOL−CHOL association.

Can $\beta\beta$ cholesterol dimers also mediate membrane protein function? Although direct experimental data are scarce, recent structural studies of the amyloid precursor protein (APP) in a membrane-mimetic environment suggest such a potential interaction. Perturbations to the solution NMR chemical shifts of C99 in response to changing cholesterol concentrations suggested a direct interaction of cholesterol with C99 in detergent micelles and bicelles.[73−75] Cholesterol was found to interact weakly with C99, which may inhibit C99 homodimerization.[76] Recent MD simulations suggested that cholesterol interacts with C99 at multiple specific sites that differ from the nonspecific lipid interaction sites.[77] Some of these specific C99−CHOL interactions employ the cholesterol β face. It was also demonstrated that the C99 structure is affected by the induction of the L_o phase by cholesterol. It was hypothesized that this weak C99−CHOL interaction may be responsible for facilitating the APP−β-secretase and C99−γ-secretase interactions that ultimately produce the amyloid-β peptide in the amyloid cascade hypothesis of Alzheimer's disease,[78] by bringing C99 to L_o domains in which these secretases reside.[79,80]

Regardless of the relative populations of $\alpha\alpha$ and $\beta\beta$ cholesterol dimers in the lipid membrane, these small cholesterol dimers and tetramers could serve as the "glue" to mediate protein−protein interactions in lipid bilayers.[81,82] Such a regulatory role has been proposed for the β2 adrenergic receptor,[11] the mitochondrial translocator protein TSPO,[82] the μ-opioid receptor,[83,84] and the chemokine receptor CXCR4.[85] Emerging experimental evidence also suggests that the protein association promoted by cholesterol oligomers may have functional consequences. For example, the influenza M2 protein binds the β face of cholesterol to be recruited to the edge of the virus budozone, where it causes membrane curvature, which is required for membrane scission and virus release.[23,86,87] If the basic unit of cholesterol is a dimer instead of a monomer in the plasma membrane, then the cholesterol dimers could help to recruit multiple M2 tetramers to the neck of the budding virus, thus amplifying the membrane curvature. Indeed, M2 clustering has been recently reported based on ^{2}H NMR data that show slowed methyl dynamics of lipid-facing alanine residues.[88,89] Future investigations of the molecular structures of cholesterol−protein interactions will be important to provide further examples of how cholesterol oligomerization mediates protein−protein interactions.

■ ASSOCIATED CONTENT

Supporting Information

The Supporting Information is available free of charge at https://pubs.acs.org/doi/10.1021/acs.jpcb.0c10631.

Cholesterol chemical shifts, membrane samples used in this study, intermolecular correlation peaks, crystal structures of cholesterol-containing membrane proteins, and NMR spectra and MD simulation results (PDF)

■ AUTHOR INFORMATION

Corresponding Authors

John E. Straub − *Department of Chemistry, Boston University, Boston, Massachusetts 02215, United States;* orcid.org/0000-0002-2355-3316; Email: straub@bu.edu

https://dx.doi.org/10.1021/acs.jpcb.0c10631
J. Phys. Chem. B XXXX, XXX, XXX−XXX

Mei Hong − *Department of Chemistry, Massachusetts Institute of Technology, Cambridge, Massachusetts 02139, United States;* orcid.org/0000-0001-5255-5858; Email: meihong@mit.edu

Authors

Matthew R. Elkins − *Department of Chemistry, Massachusetts Institute of Technology, Cambridge, Massachusetts 02139, United States*

Asanga Bandara − *Department of Chemistry, Boston University, Boston, Massachusetts 02215, United States*

George A. Pantelopulos − *Department of Chemistry, Boston University, Boston, Massachusetts 02215, United States;* orcid.org/0000-0002-4373-1677

Complete contact information is available at: https://pubs.acs.org/10.1021/acs.jpcb.0c10631

Notes

The authors declare no competing financial interest.

■ ACKNOWLEDGMENTS

This research is supported by National Institutes of Health grant GM088204 to M.H. and GM107703 to J.E.S. The authors thank Prof. Howard Riezman and Brigitte Bernadets for providing *S. cerevisiae* strain RH6829. This study made use of NMR spectrometers at the MIT-Harvard Center for Magnetic Resonance, which is supported by NIH grant P41 GM132079.

■ REFERENCES

(1) Gerl, M. J.; Sampaio, J. L.; Urban, S.; Kalvodova, L.; Verbavatz, J.-M.; Binnington, B.; Lindemann, D.; Lingwood, C. A.; Shevchenko, A.; Schroeder, C.; et al. Quantitative analysis of the lipidomes of the influenza virus envelope and MDCK cell apical membrane. *J. Cell Biol.* **2012**, *196*, 213−221.

(2) Dawidowicz, E. A. Dynamics of membrane lipid metabolism and turnover. *Annu. Rev. Biochem.* **1987**, *56*, 43−57.

(3) Levitan, I.; Singh, D. K.; Rosenhouse-Dantsker, A. Cholesterol binding to ion channels. *Front. Physiol.* **2014**, *5*, 65.

(4) Oates, J.; Watts, A. Uncovering the intimate relationship between lipids, cholesterol and GPCR activation. *Curr. Opin. Struct. Biol.* **2011**, *21*, 802−807.

(5) Fantini, J.; Barrantes, F. J. How cholesterol interacts with membrane proteins: an exploration of cholesterol-binding sites including CRAC, CARC, and tilted domains. *Front. Physiol.* **2013**, *4*, 31.

(6) Veatch, S. L.; Keller, S. L. Seeing spots: complex phase behavior in simple membranes. *Biochim. Biophys. Acta* **2005**, *1746*, 172−185.

(7) Bartels, T.; Lankalapalli, R. S.; Bittman, R.; Beyer, K.; Brown, M. F. Raftlike mixtures of sphingomyelin and cholesterol investigated by solid-state 2H NMR spectroscopy. *J. Am. Chem. Soc.* **2008**, *130*, 14521−14532.

(8) Marsh, D. Liquid-ordered phases induced by cholesterol: A compendium of binary phase diagrams. *Biochim. Biophys. Acta Biomembr.* **2010**, *1798*, 688−699.

(9) Lingwood, D.; Simons, K. Lipid rafts as a membrane-organizing principle. *Science* **2010**, *327*, 46−50.

(10) Jacobson, K.; Mouritsen, O. G.; Anderson, R. G. W. Lipid rafts: at a crossroad between cell biology and physics. *Nat. Cell Biol.* **2007**, *9*, 7−14.

(11) Hanson, M. A.; Cherezov, V.; Griffith, M. T.; Roth, C. B.; Jaakola, V.-P.; Chien, E. Y. T.; Velasquez, J.; Kuhn, P.; Stevens, R. C. A specific cholesterol binding site is established by the 2.8 A structure of the human beta2-adrenergic receptor. *Structure* **2008**, *16*, 897−905.

(12) Lai, A. L.; Moorthy, A. E.; Li, Y.; Tamm, L. K. Fusion activity of HIV gp41 fusion domain is related to its secondary structure and depth of membrane insertion in a cholesterol-dependent fashion. *J. Mol. Biol.* **2012**, *418*, 3−15.

(13) Maxfield, F. R.; Tabas, I. Role of cholesterol and lipid organization in disease. *Nature* **2005**, *438*, 612−621.

(14) Martin, R. B.; Yeagle, P. L. Models for lipid organization in cholesterol-phospholipid bilayers including cholesterol dimer formation. *Lipids* **1978**, *13*, 594−597.

(15) Bandara, A.; Panahi, A.; Pantelopulos, G. A.; Straub, J. E. Exploring the structure and stability of cholesterol dimer formation in multicomponent lipid bilayers. *J. Comput. Chem.* **2017**, *38*, 1479−1488.

(16) Harris, J. S.; Epps, D. E.; Davio, S. R.; Kezdy, F. J. Evidence for transbilayer, tail-to-tail cholesterol dimers in dipalmitoylglycerophosphocholine liposomes. *Biochemistry* **1995**, *34*, 3851−3857.

(17) Mukherjee, S.; Chattopadhyay, A. Membrane organization at low cholesterol concentrations: a study using 7-nitrobenz-2-oxa-1,3-diazol-4-yl-labeled cholesterol. *Biochemistry* **1996**, *35*, 1311−1322.

(18) Dufourc, E. J.; Smith, I. C. P. A detailed analysis of the motions of cholesterol in biological membranes by 2H-NMR relaxation. *Chem. Phys. Lipids* **1986**, *41*, 123−135.

(19) Aussenac, F.; Tavares, M.; Dufourc, E. J. Cholesterol dynamics in membranes of raft composition: a molecular point of view from 2H and 31P solid-state NMR. *Biochemistry* **2003**, *42*, 1383−1390.

(20) Souza, C. M.; Schwabe, T. M. E.; Pichler, H.; Ploier, B.; Leitner, E.; Guan, X. L.; Wenk, M. R.; Riezman, I.; Riezman, H. A stable yeast strain efficiently producing cholesterol instead of ergosterol is functional for tryptophan uptake, but not weak organic acid resistance. *Metab. Eng.* **2011**, *13*, 555−569.

(21) Shivapurkar, R.; Souza, C. M.; Jeannerat, D.; Riezman, H. An efficient method for the production of isotopically enriched cholesterol for NMR. *J. Lipid Res.* **2011**, *52*, 1062−1065.

(22) Della Ripa, L. A.; Petros, Z. A.; Cioffi, A. G.; Piehl, D. W.; Courtney, J. M.; Burke, M. D.; Rienstra, C. M. Solid-State NMR of highly (13)C-enriched cholesterol in lipid bilayers. *Methods* **2018**, *138*−*139*, 47−53.

(23) Elkins, M. R.; Sergeyev, I. V.; Hong, M. Determining Cholesterol Binding to Membrane Proteins by Cholesterol 13C Labeling in Yeast and Dynamic Nuclear Polarization NMR. *J. Am. Chem. Soc.* **2018**, *140*, 15437−15449.

(24) Cady, S.; Wang, T.; Hong, M. Membrane-dependent effects of a cytoplasmic helix on the structure and drug binding of the influenza virus M2 protein. *J. Am. Chem. Soc.* **2011**, *133*, 11572−11579.

(25) Luo, W.; Cady, S. D.; Hong, M. Immobilization of the Influenza A M2 Transmembrane Peptide in Virus-Envelope Mimetic Lipid Membranes: A Solid-State NMR Investigation. *Biochemistry* **2009**, *48*, 6361−6368.

(26) Brügger, B.; Glass, B.; Haberkant, P.; Leibrecht, I.; Wieland, F. T.; Kräusslich, H.-G. The HIV lipidome: a raft with an unusual composition. *Proc. Natl. Acad. Sci. U.S.A.* **2006**, *103*, 2641−2646.

(27) van Meer, G.; Voelker, D. R.; Feigenson, G. W. Membrane lipids: where they are and how they behave. *Nat. Rev. Mol. Cell Biol.* **2008**, *9*, 112−124.

(28) Hou, G. J.; Yan, S.; Trébosc, J.; Amoureux, J. P.; Polenova, T. Broadband homonuclear correlation spectroscopy driven by combined R2(n)(v) sequences under fast magic angle spinning for NMR structural analysis of organic and biological solids. *J. Magn. Reson.* **2013**, *232*, 18−30.

(29) deAzevedo, E. R.; Hu, W.-G.; Bonagamba, T. J.; Schmidt-Rohr, K. Centerband-only detection of exchange: Efficient analysis of dynamics in solids by NMR. *J. Am. Chem. Soc.* **1999**, *121*, 8411−8412.

(30) Buffy, J. J.; Waring, A. J.; Hong, M. Determination of peptide oligomerization in lipid bilayers using 19F spin diffusion NMR. *J. Am. Chem. Soc.* **2005**, *127*, 4477−4483.

(31) Luo, W.; Hong, M. Determination of the oligomeric number and intermolecular distances of membrane protein assemblies by anisotropic 1H-driven spin diffusion NMR spectroscopy. *J. Am. Chem. Soc.* **2006**, *128*, 7242−7251.

(32) Elkins, M. R.; Williams, J. K.; Gelenter, M. D.; Dai, P.; Kwon, B.; Sergeyev, I. V.; Pentelute, B. L.; Hong, M. Cholesterol-binding site

of the influenza M2 protein in lipid bilayers from solid-state NMR. *Proc. Natl. Acad. Sci. U.S.A.* **2017**, *114*, 12946−12951.
(33) Pantelopulos, G. A.; Nagai, T.; Bandara, A.; Panahi, A.; Straub, J. E. Critical size dependence of domain formation observed in coarse-grained simulations of bilayers composed of ternary lipid mixtures. *J. Chem. Phys.* **2017**, *147*, 095101.
(34) Abraham, M. J.; Murtola, T.; Schulz, R.; Páll, S.; Smith, J. C.; Hess, B.; Lindahl, E. Gromacs: High performance molecular simulations through multi-level parallelism from laptops to supercomputers. *SoftwareX* **2015**, *1−2*, 19−25.
(35) Klauda, J. B.; Venable, R. M.; Freites, J. A.; O'Connor, J. W.; Tobias, D. J.; Mondragon-Ramirez, C.; Vorobyov, I.; MacKerell, A. D.; Pastor, R. W. Update of the CHARMM All-Atom Additive Force Field for Lipids: Validation on Six Lipid Types. *J. Phys. Chem. B* **2010**, *114*, 7830−7843.
(36) Jorgensen, W. L.; Chandrasekhar, J.; Madura, J. D.; Impey, R. W.; Klein, M. L. Comparison of simple potential functions for simulating liquid water. *J. Chem. Phys.* **1983**, *79*, 926−935.
(37) Jo, S.; Cheng, X.; Lee, J.; Kim, S.; Park, S.-J.; Patel, D. S.; Beaven, A. H.; Lee, K. I.; Rui, H.; Park, S.; et al. CHARMM-GUI 10 years for biomolecular modeling and simulation. *J. Comput. Chem.* **2017**, *38*, 1114−1124.
(38) Jo, S.; Kim, T.; Iyer, V. G.; Im, W. CHARMM-GUI: A web-based graphical user interface for CHARMM. *J. Comput. Chem.* **2008**, *29*, 1859−1865.
(39) Wu, E. L.; Cheng, X.; Jo, S.; Rui, H.; Song, K. C.; Dávila-Contreras, E. M.; Qi, Y.; Lee, J.; Monje-Galvan, V.; Venable, R. M.; et al. CHARMM-GUI Membrane Builder toward realistic biological membrane simulations. *J. Comput. Chem.* **2014**, *35*, 1997−2004.
(40) Hess, B. P-LINCS: A Parallel Linear Constraint Solver for Molecular Simulation. *J. Chem. Theory Comput.* **2008**, *4*, 116−122.
(41) Hoover, W. G. Canonical dynamics: Equilibrium phase-space distributions. *Phys. Rev. A* **1985**, *31*, 1695−1697.
(42) Nosé, S. A unified formulation of the constant temperature molecular dynamics methods. *J. Chem. Phys.* **1984**, *81*, 511−519.
(43) Parrinello, M.; Rahman, A. Polymorphic transitions in single crystals: A new molecular dynamics method. *J. Appl. Physiol.* **1981**, *52*, 7182−7190.
(44) Essmann, U.; Perera, L.; Berkowitz, M. L.; Darden, T.; Lee, H.; Pedersen, L. G. A smooth particle mesh Ewald method. *J. Chem. Phys.* **1995**, *103*, 8577−8593.
(45) Humphrey, W.; Dalke, A.; Schulten, K. VMD: Visual molecular dynamics. *J. Mol. Graph.* **1996**, *14*, 33−38.
(46) Gowers, R.; Linke, M.; Barnoud, J.; Reddy, T.; Melo, M.; Seyler, S.; Domański, J.; Dotson, D.; Buchoux, S.; Kenney, I., et al. MDAnalysis: A Python Package for the Rapid Analysis of Molecular Dynamics Simulations. *Proceedings of the 15th Python in Science Conference*, 2018; pp 98−105.
(47) Michaud-Agrawal, N.; Denning, E. J.; Woolf, T. B.; Beckstein, O. MDAnalysis: A toolkit for the analysis of molecular dynamics simulations. *J. Comput. Chem.* **2011**, *32*, 2319−2327.
(48) Pantelopulos, G. A.; Straub, J. E. Regimes of Complex Lipid Bilayer Phases Induced by Cholesterol Concentration in MD Simulation. *Biophys. J.* **2018**, *115*, 2167−2178.
(49) Park, S.; Im, W. Quantitative Characterization of Cholesterol Partitioning between Binary Bilayers. *J. Chem. Theory Comput.* **2018**, *14*, 2829−2833.
(50) Chen, L.; Yu, Z.; Quinn, P. J. The partition of cholesterol between ordered and fluid bilayers of phosphatidylcholine: a synchrotron X-ray diffraction study. *Biochim. Biophys. Acta* **2007**, *1768*, 2873−2881.
(51) Soteras Gutiérrez, I.; Lin, F.-Y.; Vanommeslaeghe, K.; Lemkul, J. A.; Armacost, K. A.; Brooks, C. L.; MacKerell, A. D. Parametrization of halogen bonds in the CHARMM general force field: Improved treatment of ligand−protein interactions. *Bioorg. Med. Chem.* **2016**, *24*, 4812−4825.
(52) Vanommeslaeghe, K.; Hatcher, E.; Acharya, C.; Kundu, S.; Zhong, S.; Shim, J.; Darian, E.; Guvench, O.; Lopes, P.; Vorobyov, I.; et al. CHARMM general force field: A force field for drug-like molecules compatible with the CHARMM all-atom additive biological force fields. *J. Comput. Chem.* **2009**, *31*, 671.
(53) Vanommeslaeghe, K.; MacKerell, A. D. Automation of the CHARMM General Force Field (CGenFF) I: Bond Perception and Atom Typing. *J. Chem. Inf. Model.* **2012**, *52*, 3144−3154.
(54) Vanommeslaeghe, K.; Raman, E. P.; MacKerell, A. D. Automation of the CHARMM General Force Field (CGenFF) II: Assignment of Bonded Parameters and Partial Atomic Charges. *J. Chem. Inf. Model.* **2012**, *52*, 3155−3168.
(55) Yu, W.; He, X.; Vanommeslaeghe, K.; MacKerell, A. D. Extension of the CHARMM general force field to sulfonyl-containing compounds and its utility in biomolecular simulations. *J. Comput. Chem.* **2012**, *33*, 2451−2468.
(56) Lim, J. B.; Rogaski, B.; Klauda, J. B. Update of the Cholesterol Force Field Parameters in CHARMM. *J. Phys. Chem. B* **2012**, *116*, 203−210.
(57) Ando, T.; Skolnick, J. Crowding and hydrodynamic interactions likely dominate in vivo macromolecular motion. *Proc. Natl. Acad. Sci. U.S.A.* **2010**, *107*, 18457−18462.
(58) Kauffman, J. M.; Westerman, P. W.; Carey, M. C. Fluorocholesterols, in contrast to hydroxycholesterols, exhibit interfacial properties similar to cholesterol. *J. Lipid Res.* **2000**, *41*, 991−1003.
(59) Toppozini, L.; Meinhardt, S.; Armstrong, C. L.; Yamani, Z.; Kučerka, N.; Schmid, F.; Rheinstädter, M. C. Structure of Cholesterol in Lipid Rafts. *Phys. Rev. Lett.* **2014**, *113*, 228101.
(60) Dai, J.; Alwarawrah, M.; Huang, J. Instability of cholesterol clusters in lipid bilayers and the cholesterol's Umbrella effect. *J. Phys. Chem. B* **2010**, *114*, 840−848.
(61) Alwarawrah, M.; Dai, J.; Huang, J. A molecular view of the cholesterol condensing effect in DOPC lipid bilayers. *J. Phys. Chem. B* **2010**, *114*, 7516−7523.
(62) Leeb, F.; Maibaum, L. Spatially Resolving the Condensing Effect of Cholesterol in Lipid Bilayers. *Biophys. J.* **2018**, *115*, 2179−2188.
(63) Huang, J.; Buboltz, J. T.; Feigenson, G. W. Maximum solubility of cholesterol in phosphatidylcholine and phosphatidylethanolamine bilayers. *Biochim. Biophys. Acta* **1999**, *1417*, 89−100.
(64) Marrink, S. J.; Corradi, V.; Souza, P. C. T.; Ingólfsson, H. I.; Tieleman, D. P.; Sansom, M. S. P. Computational Modeling of Realistic Cell Membranes. *Chem. Rev.* **2019**, *119*, 6184−6226.
(65) Huang, J.; Feigenson, G. W. A microscopic interaction model of maximum solubility of cholesterol in lipid bilayers. *Biophys. J.* **1999**, *76*, 2142−2157.
(66) Ali, M. R.; Cheng, K. H.; Huang, J. Assess the nature of cholesterol-lipid interactions through the chemical potential of cholesterol in phosphatidylcholine bilayers. *Proc. Natl. Acad. Sci. U.S.A.* **2007**, *104*, 5372−5377.
(67) Sodt, A. J.; Sandar, M. L.; Gawrisch, K.; Pastor, R. W.; Lyman, E. The molecular structure of the liquid-ordered phase of lipid bilayers. *J. Am. Chem. Soc.* **2014**, *136*, 725−732.
(68) Sodt, A. J.; Pastor, R. W.; Lyman, E. Hexagonal Substructure and Hydrogen Bonding in Liquid-Ordered Phases Containing Palmitoyl Sphingomyelin. *Biophys. J.* **2015**, *109*, 948−955.
(69) Miao, L.; Nielsen, M.; Thewalt, J.; Ipsen, J. H.; Bloom, M.; Zuckermann, M. J.; Mouritsen, O. G. From lanosterol to cholesterol: structural evolution and differential effects on lipid bilayers. *Biophys. J.* **2002**, *82*, 1429−1444.
(70) Nishio, M.; Umezawa, Y.; Hirota, M.; Takeuchi, Y. Tetrahedron Report Number-378-the Ch/Pi Interaction - Significance in Molecular Recognition. *Tetrahedron* **1995**, *51*, 8665−8701.
(71) Ounjian, J.; Bukiya, A. N.; Rosenhouse-Dantsker, A. Molecular Determinants of Cholesterol Binding to Soluble and Transmembrane Protein Domains. *Adv. Exp. Med. Biol.* **2019**, *1135*, 47−66.
(72) Wang, C.; Ralko, A.; Ren, Z.; Rosenhouse-Dantsker, A.; Yang, X. Modes of Cholesterol Binding in Membrane Proteins: A Joint Analysis of 73 Crystal Structures. In *Direct Mechanisms in Cholesterol Modulation of Protein Function*; Rosenhouse-Dantsker, A., Bukiya, A. N., Eds.; Springer International Publishing: Cham, 2019; pp 67−88.

https://dx.doi.org/10.1021/acs.jpcb.0c10631
J. Phys. Chem. B XXXX, XXX, XXX−XXX

(73) Barrett, P. J.; Song, Y.; Van Horn, W. D.; Schafer, J. M.; Hadziselimovic, A.; Beel, A. J.; Sanders, C. R. The amyloid precursor protein has a flexible transmembrane domain and binds cholesterol. *Science* **2012**, *336*, 1168−1171.
(74) Song, Y.; Hustedt, E. J.; Brandon, S.; Sanders, C. R. Competition between homodimerization and cholesterol binding to the C99 domain of the amyloid precursor protein. *Biochemistry* **2013**, *52*, 5051−5064.
(75) Song, Y.; Mittendorf, K. F.; Lu, Z.; Sanders, C. R. Impact of bilayer lipid composition on the structure and topology of the transmembrane amyloid precursor C99 protein. *J. Am. Chem. Soc.* **2014**, *136*, 4093−4096.
(76) Panahi, A.; Bandara, A.; Pantelopulos, G. A.; Dominguez, L.; Straub, J. E. Specific Binding of Cholesterol to C99 Domain of Amyloid Precursor Protein Depends Critically on Charge State of Protein. *J. Phys. Chem. Lett.* **2016**, *7*, 3535−3541.
(77) Pantelopulos, G. A.; Panahi, A.; Straub, J. E. Impact of Cholesterol Concentration and Lipid Phase on Structure and Fluctuation of Amyloid Precursor Protein. *J. Phys. Chem. B* **2020**, *124*, 10173−10185.
(78) Hicks, D. A.; Nalivaeva, N. N.; Turner, A. J. Lipid rafts and Alzheimer's disease: protein-lipid interactions and perturbation of signaling. *Front. Physiol.* **2012**, *3*, 189.
(79) Montesinos, J.; Pera, M.; Larrea, D.; Guardia-Laguarta, C.; Agrawal, R. R.; Velasco, K. R.; Yun, T. D.; Stavrovskaya, I. G.; Xu, Y.; Koo, S. Y.; et al. The Alzheimer's disease-associated C99 fragment of APP regulates cellular cholesterol trafficking. *EMBO J.* **2020**, *39*, No. e103791.
(80) Song, Y.; Kenworthy, A. K.; Sanders, C. R. Cholesterol as a co-solvent and a ligand for membrane proteins. *Protein Sci.* **2014**, *23*, 1−22.
(81) Prasanna, X.; Chattopadhyay, A.; Sengupta, D. Cholesterol modulates the dimer interface of the beta(2)-adrenergic receptor via cholesterol occupancy sites. *Biophys. J.* **2014**, *106*, 1290−1300.
(82) Jaipuria, G.; Leonov, A.; Giller, K.; Vasa, S. K.; Jaremko, L.; Jaremko, M.; Linser, R.; Becker, S.; Zweckstetter, M. Cholesterol-mediated allosteric regulation of the mitochondrial translocator protein structure. *Nat. Commun.* **2017**, *8*, 14893.
(83) Manglik, A.; Kruse, A. C.; Kobilka, T. S.; Thian, F. S.; Mathiesen, J. M.; Sunahara, R. K.; Pardo, L.; Weis, W. I.; Kobilka, B. K.; Granier, S. Crystal structure of the μ-opioid receptor bound to a morphinan antagonist. *Nature* **2012**, *485*, 321−326.
(84) Huang, W.; Manglik, A.; Venkatakrishnan, A. J.; Laeremans, T.; Feinberg, E. N.; Sanborn, A. L.; Kato, H. E.; Livingston, K. E.; Thorsen, T. S.; Kling, R. C.; et al. Structural insights into micro-opioid receptor activation. *Nature* **2015**, *524*, 315−321.
(85) Pluhackova, K.; Gahbauer, S.; Kranz, F.; Wassenaar, T. A.; Böckmann, R. A. Dynamic Cholesterol-Conditioned Dimerization of the G Protein Coupled Chemokine Receptor Type 4. *PLoS Comput. Biol.* **2016**, *12*, No. e1005169.
(86) Rossman, J. S.; Jing, X.; Leser, G. P.; Lamb, R. A. Influenza virus M2 protein mediates ESCRT-independent membrane scission. *Cell* **2010**, *142*, 902−913.
(87) Schmidt, N. W.; Mishra, A.; Wang, J.; DeGrado, W. F.; Wong, G. C. L. Influenza virus A M2 protein generates negative Gaussian membrane curvature necessary for budding and scission. *J. Am. Chem. Soc.* **2013**, *135*, 13710−13719.
(88) Paulino, J.; Pang, X.; Hung, I.; Zhou, H.-X.; Cross, T. A. Influenza A M2 Channel Clustering at High Protein/Lipid Ratios: Viral Budding Implications. *Biophys. J.* **2019**, *116*, 1075−1084.
(89) Andreas, L. B.; Reese, M.; Eddy, M. T.; Gelev, V.; Ni, Q. Z.; Miller, E. A.; Emsley, L.; Pintacuda, G.; Chou, J. J.; Griffin, R. G. Structure and Mechanism of the Influenza A M218-60 Dimer of Dimers. *J. Am. Chem. Soc.* **2015**, *137*, 14877−14886.

https://dx.doi.org/10.1021/acs.jpcb.0c10631
J. Phys. Chem. B XXXX, XXX, XXX−XXX

Supporting Information

Direct Observation of Cholesterol Dimers and Tetramers in Lipid Bilayers

Matthew R. Elkins [1], Asanga Bandara [2], George A. Pantelopulos [2], John E. Straub [2]*, Mei Hong [1]*

[1] Department of Chemistry, Massachusetts Institute of Technology, 170 Albany Street, Cambridge, MA 02139

[2] Department of Chemistry, Boston University, 590 Commonwealth Ave, Boston, MA 02215

* Corresponding authors:
Mei Hong: meihong@mit.edu
John E. Straub, straub@bu.edu

Table S1. Membrane samples used to measure cholesterol self-association in this study.

Membrane composition	CHOL concentration	CHOL labeling	SSNMR experiments
VM+ (POPC : POPE : PSM : CHOL) 27.7 : 27.7 : 27.7% : 17%	17%	F7-CHOL	1D and 2D FF, 2D ^{19}F CODEX
VM+ (POPC : POPE : PSM : CHOL) 26.7 : 26.7 : 26.7% : 20%	20%	1-^{13}C CHOL and 2-^{13}C CHOL (1:1)	2D CC
VM+ (POPC : POPE : PSM : CHOL) 18.7% : 18.7% : 18.7% : 44%	44%	1-^{13}C CHOL and F7-CHOL (1:1)	2D CC
		1-^{13}C CHOL and 2-^{13}C CHOL (1:1)	2D CC
		F7-CHOL	1D and 2D FF, 2D ^{19}F CODEX
		25, 26, 27-^{13}C3-CHOL	2D ^{13}C CODEX
POPC : POPG : CHOL 66% : 17% : 17%	17%	F7-CHOL	1D ^{19}F, 2D ^{19}F CODEX
POPC : POPG : CHOL 45% : 11% : 44%	44%	F7-CHOL	1D ^{19}F, 2D ^{19}F CODEX

Table S2. CHARMM36 charges and CGenFF-generated F7-CHOL atom types, charge assignments, and charge penalties.

F7-CHOL atom name	CGenFF F7-CHOL atom type	CHARMM36 Chol charge	CGenFF F7-CHOL charge	CGenFF F7-CHOL charge score
C20	CG311	-0.090	-0.094	0.000
H20	HGA1	0.090	0.090	0.000
C21	CG331	-0.270	-0.270	0.000
H21[A-C]	HGA3	0.090	0.090	0.000
C22	CG321	-0.180	-0.193	0.600
H22[A-B]	HGA2	0.090	0.090	0.000
C23	CG321	-0.180	-0.160	4.453
H23[A-B]	HGA2	0.090	0.090	0.600
C24	CG321	-0.180	-0.096	11.374
H24[A-B]	HGA2	0.090	0.090	3.568
C25	CG322	-0.090	0.306	108.121
F25	FGA1	0.090	-0.220	6.707
C26	CG302	-0.270	0.344	76.562
F26[A-C]	FGA3	0.090	-0.140	6.586
C27	CG302	-0.270	0.344	76.562
F27[A-C]	FGA3	0.090	-0.140	6.586

Table S3. CGenFF-generated F7-Chol bond terms with non-zero penalty scores.

AT 1	Atom type 2	b_0 (nm)	k_b (kJ mol^{-1} nm^{-2})	Score
CG302	CG322	0.152	209200.0	55.0
CG321	CG322	0.152	142256.0	6.0

Table S4. CGenFF-generated F7-Chol angle and Urey-Bradley terms with non-zero penalty scores by atom types (AT).

AT 1	AT 2	AT 3	θ_0 (deg.)	k_θ (kJ mol^{-1} rad^{-2})	u_0 (nm)	k_u (kJ mol^{-1} nm^{-2})	Score
CG322	CG302	FGA3	112.0	351.456	0.2357	25104.0	12.0
CG321	CG321	CG322	113.6	488.2728	0.2561	9338.69	12.0
CG322	CG321	HGA2	110.1	289.5328	0.2179	18853.1	3.2
CG302	CG322	CG302	112.0	368.192	0.2369	25104.0	60.9
CG302	CG322	CG321	112.0	368.192	0.2369	25104.0	48.9
CG302	CG322	FGA1	112.0	368.192	0.2369	25104.0	12.9
CG321	CG322	FGA1	112.0	368.192	0.2369	25104.0	0.9

Table S5. CGenFF-generated F7-Chol proper dihedral terms with non-zero penalty scores by atom types (AT).

AT 1	AT 2	AT 3	AT 4	φ_0 (deg.)	k_φ (kJ mol^{-1}; mult.)	Score
FGA3	CG302	CG322	CG302	0.0	1.046; 3	102.0
FGA3	CG302	CG322	CG321	0.0	1.046; 3	105.5
FGA3	CG302	CG322	FGA1	0.0	1.046; 3	85.0
CG321	CG321	CG321	CG322	0.0	0.269868; 2	12.0
CG321	CG321	CG321	CG322	180.0	0.626345; 3	12.0
CG321	CG321	CG321	CG322	0.0	0.395806; 4	12.0
CG321	CG321	CG321	CG322	0.0	0.470700; 5	12.0
CG322	CG321	CG321	HGA2	0.0	0.815880; 3	12.0
CG321	CG321	CG322	CG302	0.0	0.269868; 2	67.0
CG321	CG321	CG322	CG302	180.0	0.626345; 3	67.0
CG321	CG321	CG322	CG302	0.0	0.395806; 4	67.0
CG321	CG321	CG322	CG302	0.0	0.470700; 5	67.0
CG321	CG321	CG322	FGA1	0.0	1.046000; 3	60.8
HGA2	CG321	CG322	CG302	0.0	0.774040; 3	54.0
HGA2	CG321	CG322	FGA1	0.0	0.774040; 3	6.0

Table S6. Measured ^{13}C chemical shifts of 2-^{13}C CHOL and 1-^{13}C CHOL in POPC : POPG membranes.

2-^{13}C CHOL		**1-^{13}C CHOL**	
Atom	^{13}C chemical shift (ppm)	Atom	^{13}C chemical shift (ppm)
C2	31.5	C1	38.3
C4	42.3	C3	71.4
C6	121.1	C5	142.4
C8	32.8	C7	32.7
C10	37.2	C9	50.9
C11	21.9	C13	43.1
C12	40.8	C15	25.2
C14	57.5	C17	57.5
C16	29.1	C18	12.8
C20	37.2	C19	20.2
C23	25.5	C21	19.7
C25	28.7	C22	37.3
		C24	40.4
		C26,27	23.2

Table S7. Intermolecular cholesterol correlation peaks obtained from 2D ^{13}C-^{13}C spectra measured using mixing times of 500 and 703 ms at 273 K and 750 ms at 240 K.

CHOL 1	CHOL 2	273 K	240 K
3	10	X	X
3	4		X
25	26,27		X
18	20		X
18	25		X
18	23		X
21	25		X
21	23		X
9	12		X
9	16		X

Table S8. Average residence times of the CHOL dimers identified from heavy-atom contacts in MD simulations.

System	Average dimer lifetimes (ns)		
	Inter	*Intra*	*Intra or inter*
POPC:PSM:CHOL 3:3:4 at 295 K	0.33	4.82	0.95
POPC:PSM:CHOL 4:4:2 at 295 K	0.35	4.06	0.91
POPC:PSM:CHOL 4:4:2 (phase-separated) at 295 K	0.35	4.12	0.86
POPC:PSM:F7-CHOL 3:3:4 at 295 K	0.23	6.01	0.87
POPC:PSM:F7-CHOL 4:4:2 at 295 K	0.25	3.40	0.73
POPC:PSM:CHOL 3:3:4 at 243 K	0.65	8.9	1.71
POPC:PSM:CHOL 4:4:2 at 273 K	0.47	5.82	1.19
POPC:PSM:CHOL 4:4:2 (phase-separated) at 273 K	0.43	5.80	0.96
VM+ 17% CHOL at 273 K	0.44	5.31	1.28
VM+ 17% CHOL at 243 K	0.70	7.90	1.96
VM+ 44% CHOL at 273 K	0.43	6.33	1.32
VM+ 44% CHOL at 243 K	0.67	8.15	1.94

Table S9. Analysis of integral membrane protein crystal structures with bound cholesterol. The resolution of the structures ranges from 1.45 Å to 4.3 Å. The list of protein structures was obtained from [1]. Protein-cholesterol contacts via the cholesterol α face, β face, or edge are represented by α, β, or T, respectively. "*s"* denotes simultaneous contact with α and β faces.

Protein	PDB code	No. of cholesterol	Cholesterol contact face
ATP-binding cassette G2	6HIJ	5	β, β, β, α, α
A2a adenosine receptor	5UVI	3	β, β, α
	5N2R	3	β, β, T
	5MZJ	3	β, β, T
Human β2-adrenergic receptor	3D4S	2	β, T
	3PDS	1	α
	5JQH	1	α
	5D6L	3	α, T
	5X7D	2	α, T
Na+, K+-ATPase	3KDP	1	β
	4HYT	2	β, s
	4HQJ	3	β, β, α
	4RET	2	β, s
	5AVQ	1	β
	4XE5	2	β, β
Rhodopsin AR2	3AM6	2	α, β
5-HT2B serotonin receptor	4NC3	1	β
Metabotropic glutamate receptor 1	4OR2	3	β, β, T
P2Y12 purinergic receptor	4NTJ	2	β, α
	4PXZ	1	β
GPCR homolog US28 (CX3CL1)	4XT1	2	β, α
P2Y1 purinergic receptor	4XNV	1	β
Dopamine transporter	4XNX	2	β, β
μ-opioid receptor	5C1M	1	β
ts3 serotonin receptor	5I6X	1	α
STRA6 receptor	5SY1	1	β
Tetraspanin CD81	5TCX	1	s
CC chemokine receptor type 9 (CCR9)	5LWE	1	β
	5WB2	2	α, α
Cannabinoid receptor 1 (CB1)	5XRA	1	α
Endothelin receptor B (ETB)	5X93	1	β
Multidrug resistance protein 1 (MRP1)	6BHU	3	β, β
k-opioid receptor	6B73	1	α
Cationic amino acid transporter (CAT)	5OQT	1	β

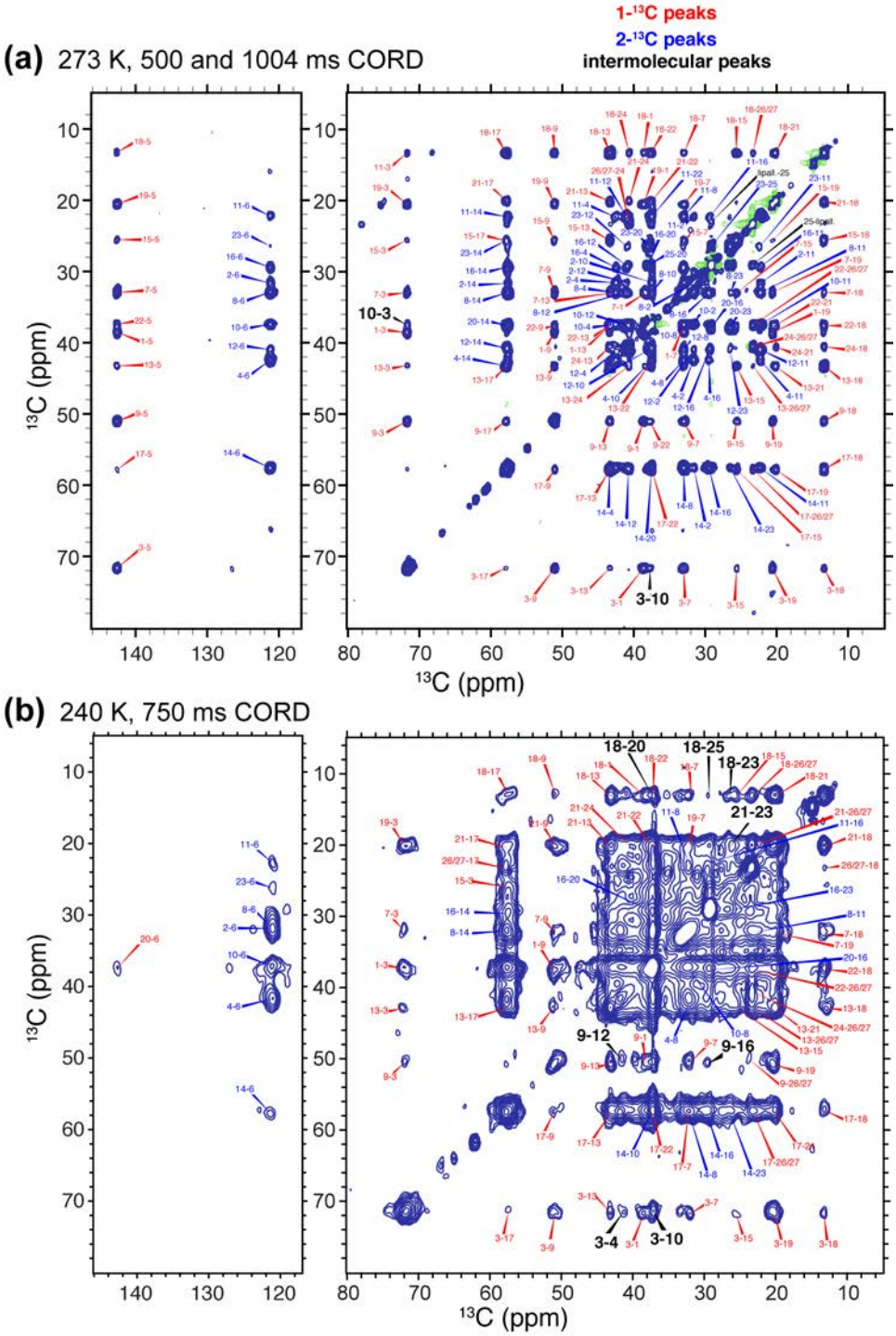

Figure S1. 2D ^{13}C-^{13}C correlation spectra of 44% mixed labeled CHOL in the VM+ membrane. 1-^{13}C and 2-^{13}C CHOL are mixed at a 1:1 ratio. (**a**) 273 K spectrum, measured using CORD mixing times of 500 ms and 1 s. Few intermolecular cross peaks are observed due to CHOL translational diffusion at this temperature. (**b**) 240 K spectrum, measured using 750 ms mixing. Many intermolecular cross peaks are observed (assigned in black).

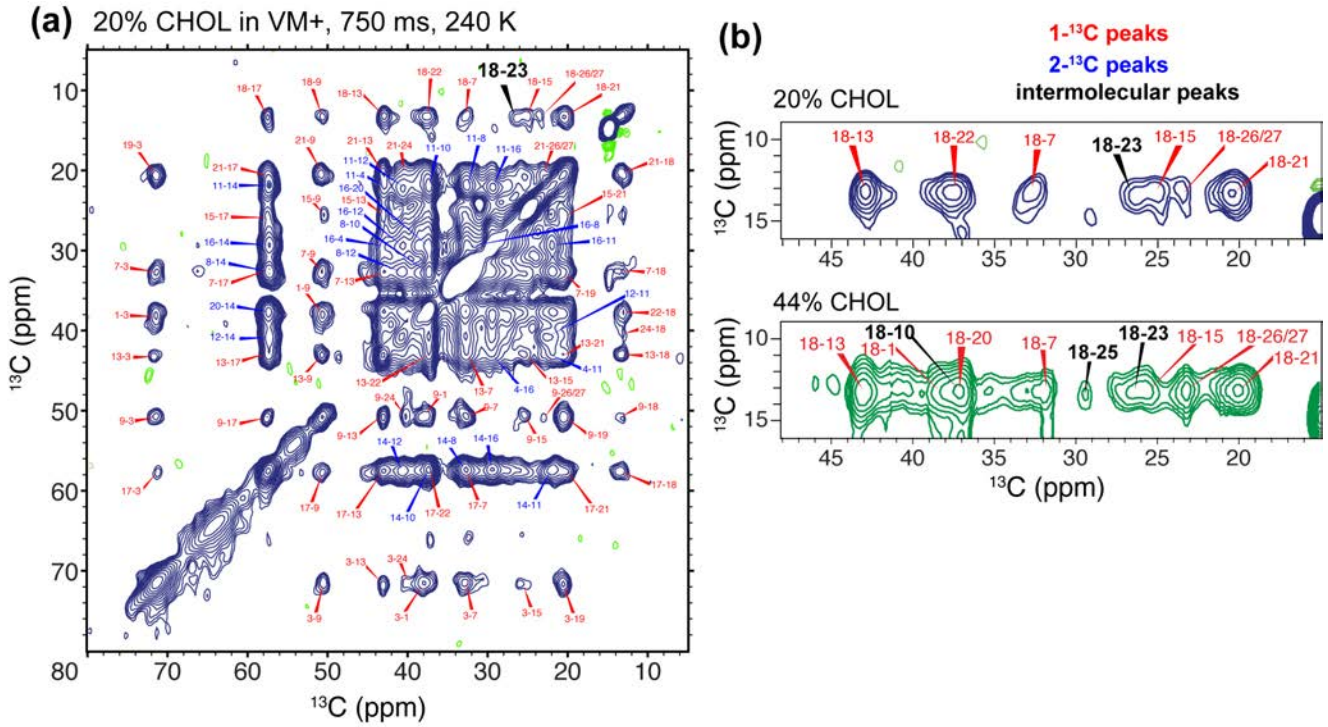

Figure S2. Intermolecular contacts of 20 mol% CHOL in the VM+ membrane. (**a**) Aliphatic region of the 2D CC spectrum of the VM+ membrane containing 1-^{13}C CHOL and 2-^{13}C CHOL mixed at a 1 : 1 ratio. The spectrum was measured at 240 K using a CORD mixing time of 750 ms. Intramolecular correlations for 1- and 2-^{13}C CHOL are marked in red and blue, while intermolecular correlations are assigned in black. (**b**) Expansion of the C18 (13 ppm) region of the 2D CC spectrum, showing an intermolecular C18–C23 correlation. The same region for the 44% CHOL sample shows additional intermolecular correlations, C18–C10 and C18–C25.

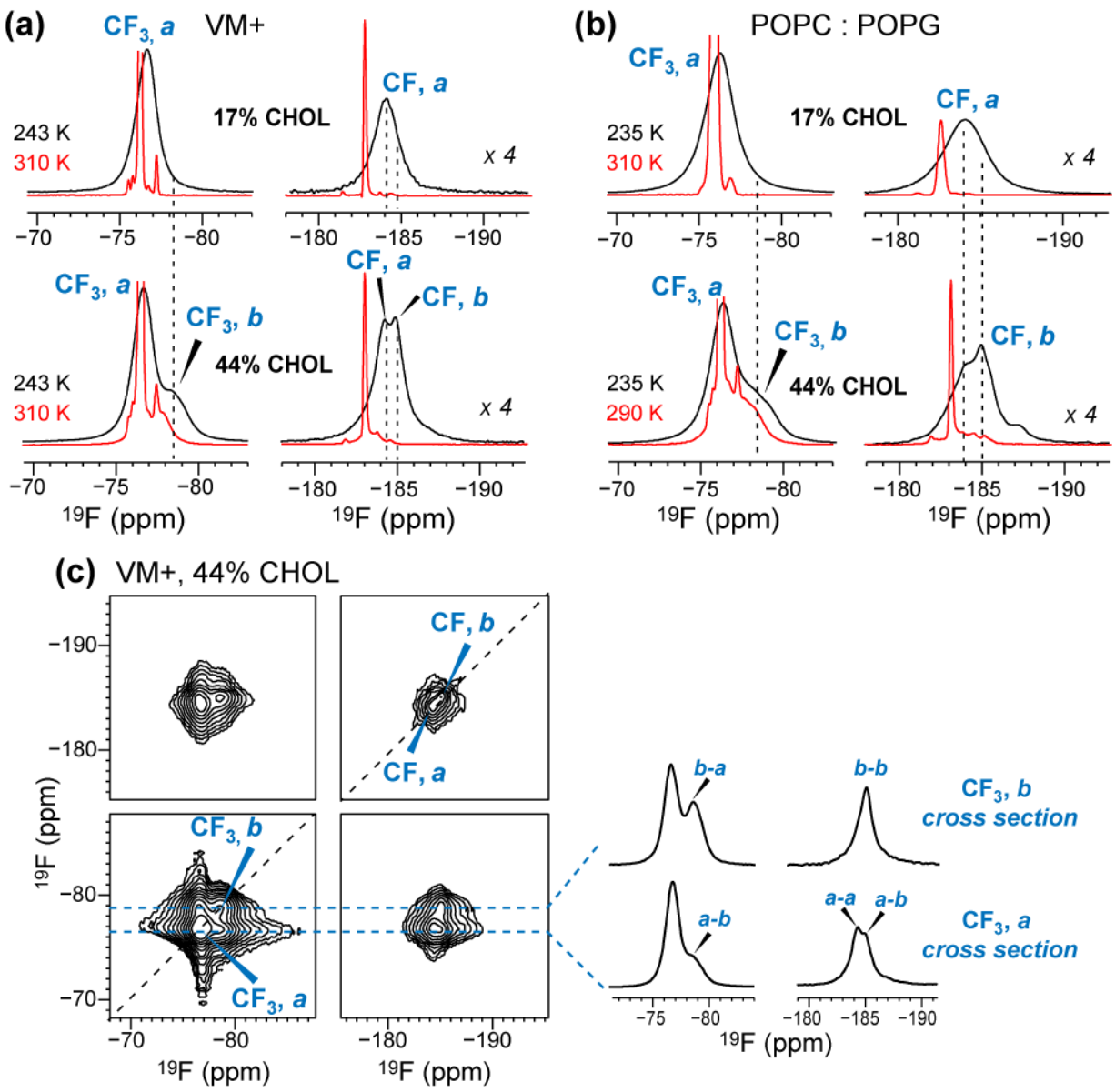

Figure S3. ^{19}F NMR spectra of F7-CHOL in lipid membranes indicate cholesterol structural heterogeneity. (a) 1D ^{19}F DP spectra of VM+ membranes containing 17% and 44% CHOL at low temperature. At 44% CHOL, a second set of CF_3 and CF peaks are observed that are absent in the 17% CHOL membranes. Spectral deconvolution of the CF_3 peaks indicates that type-*a* and type-*b* CHOL exist at 71% and 29%, respectively. (b) 1D ^{19}F DP spectra of POPC : POPG membranes containing 17% and 44% CHOL. Type-*a* and type-*b* CHOL are also observed at high CHOL concentration. (c) 2D ^{19}F-^{19}F correlation spectra of F7-CHOL in the 44% VM+ membrane. The spectra were measured at 250 K with 40 ms mixing. Both intramolecular CF_3-CF correlations and intermolecular CF_3 *a*-*b* correlations are observed, indicating that the two types of cholesterol are within nanometer contact.

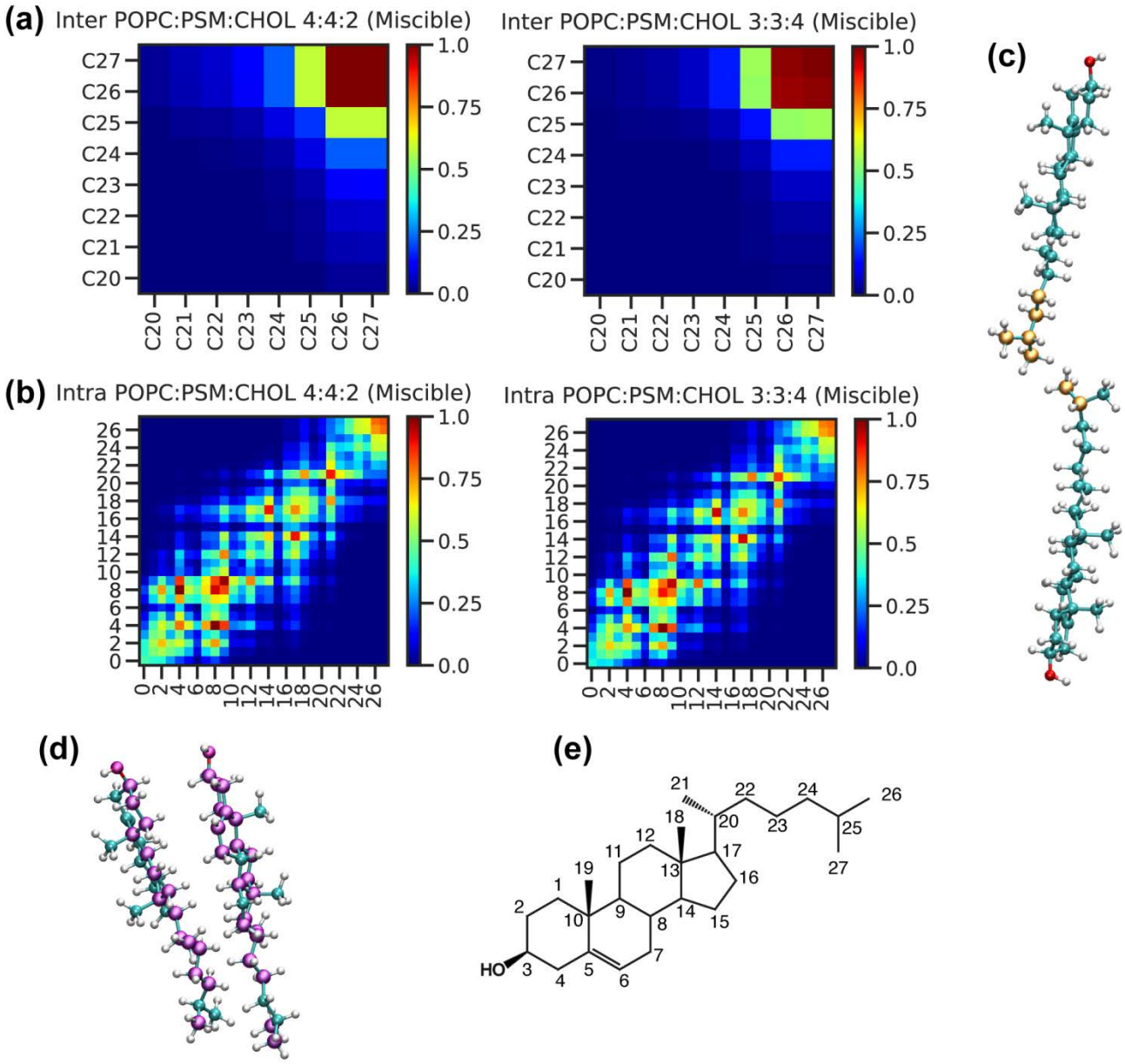

Figure S4. MD simulated contact maps for cholesterol self-association in POPC : PSM : CHOL membranes. (a) Inter-leaflet contact map in the 20% (left) and 40% (right) CHOL membranes. (b) Intra-leaflet contact map in the 20% and 40% CHOL membranes. (c) Rendering of CHOL dimers that show inter-leaflet contacts from the simulation trajectories. The heavy atoms within 5 Å of another CHOL's heavy atoms from the opposing leaflet are colored in orange. (d) Rendering of CHOL dimers that show intra-leaflet contacts from the simulation trajectories. The heavy atoms within 5 Å of another CHOL's heavy atoms are colored in purple. (e) CHOL structure showing the carbon numbering.

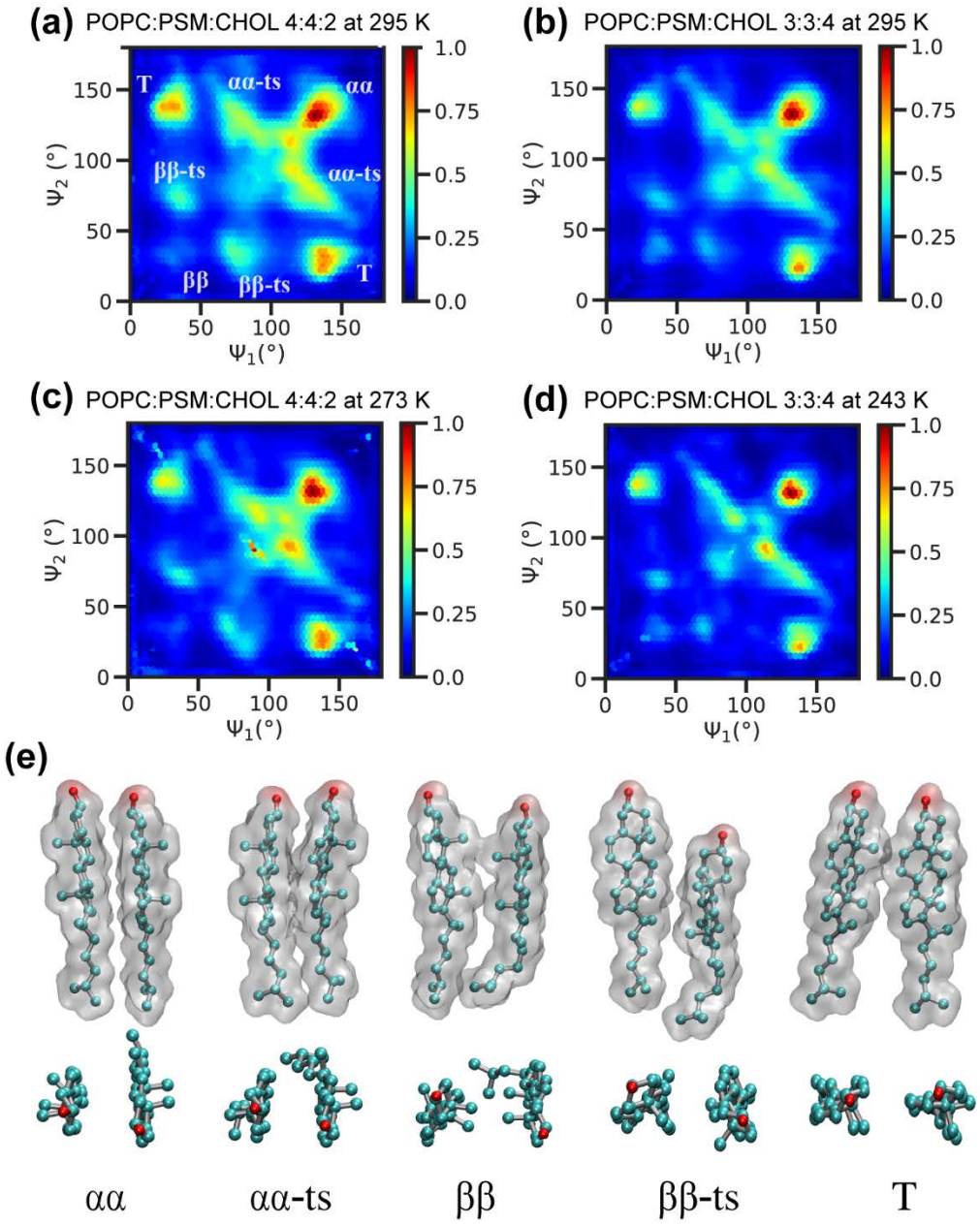

Figure S5. Simulated crick angle distributions of the instantaneous CHOL dimers in different lipid membranes at different temperatures. (a) The POPC : PSM : CHOL (3:3:4) membrane at 295 K. The dimer sub-states αα, αα-ts, ββ, ββ-ts and T are annotated. (b) The miscible POPC : PSM : CHOL (4:4:2) membrane at 295 K. (c) The POPC : PSM : CHOL (4:4:2) membrane at 273 K. (d) The POPC : PSM : CHOL (3:3:4) membrane at 243 K. (e) Side view and top view of the CHOL dimer structures for each sub-state.

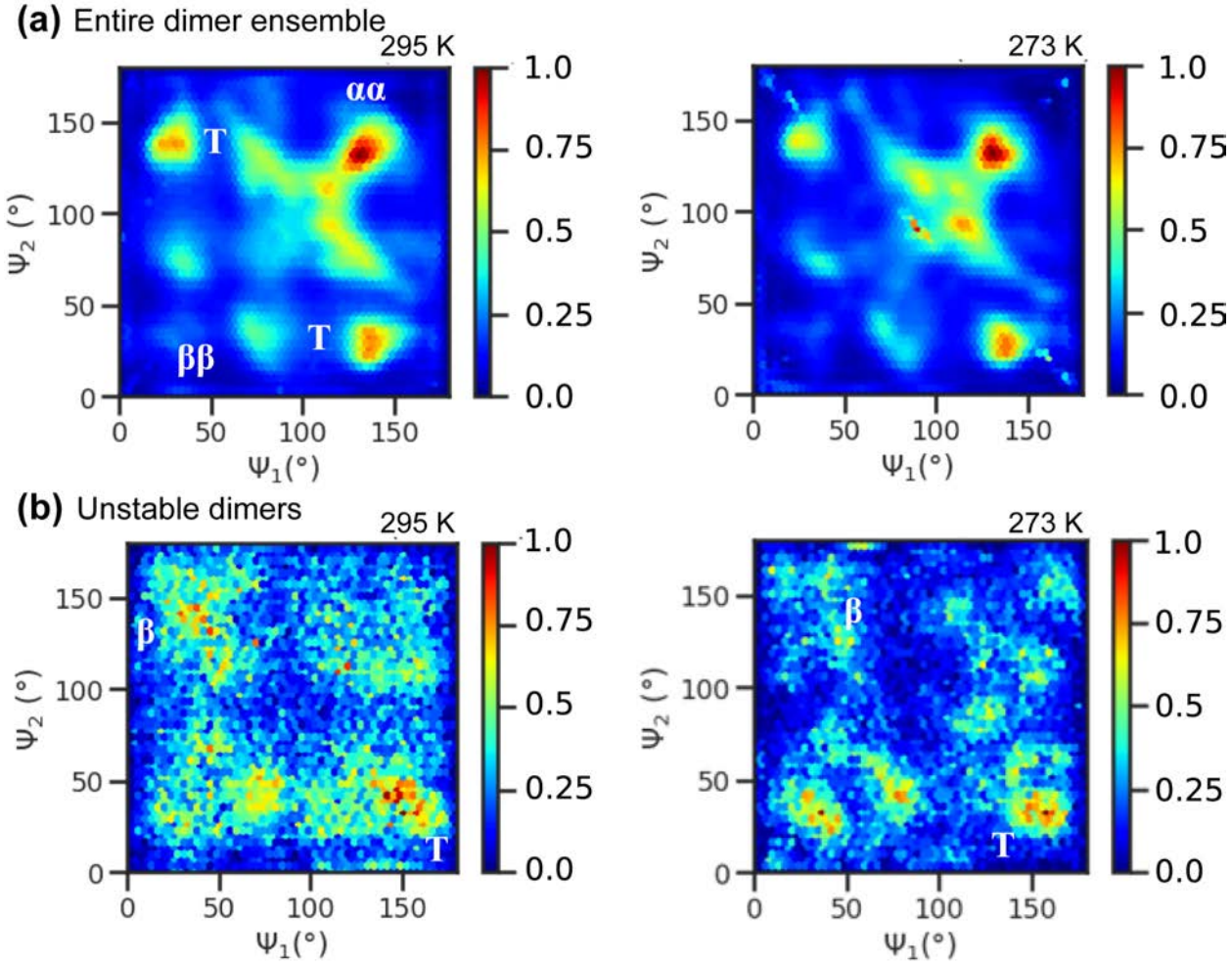

Figure S6. Simulated crick angle distributions of CHOL dimers in the miscible PSM : POPC : CHOL (4:4:2) membrane at 295 K (left) and 273 K (right). (a) The entire dimer ensemble. (b) Unstable dimers, which have residence times of less than 1 ns. The αα dimer predominates in the full dimer ensemble, whereas the T dimer predominates in the unstable dimers with short lifetimes, indicating its transient nature.

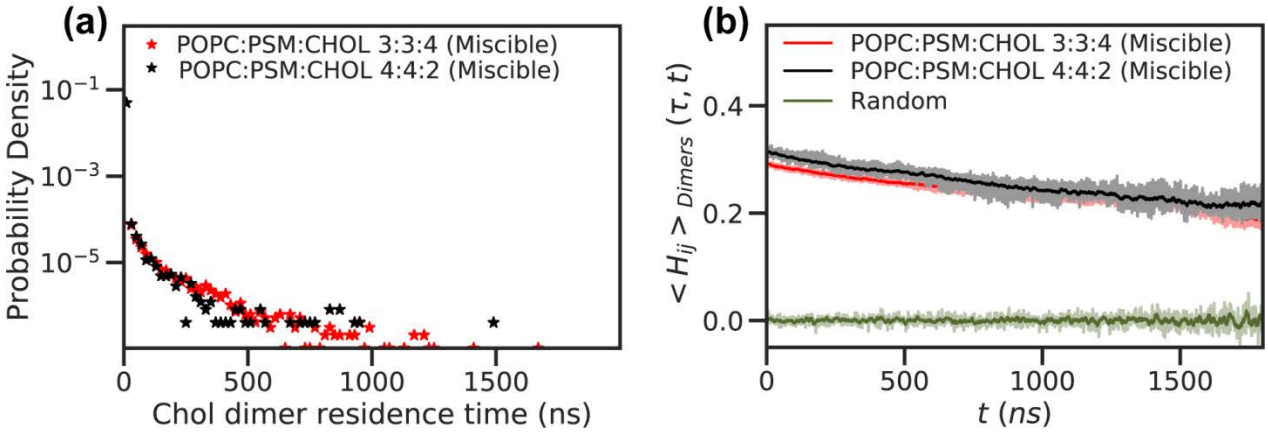

Figure S7. Simulated CHOL dimer stabilities in lipid membranes. (a) Residence time distributions of all dimers in extended (2 μs) simulation trajectories of POPC : PSM : CHOL (3:3:4) and POPC : PSM : CHOL (4:4:2) systems at 295 K. (b) Displacement pair correlation function (H_{ij}) of cholesterol dimers in the two lipid membranes. For comparison, the H_{ij} is plotted together with a randomized system. The time series are smoothed by performing a running average over a 10 ns window.

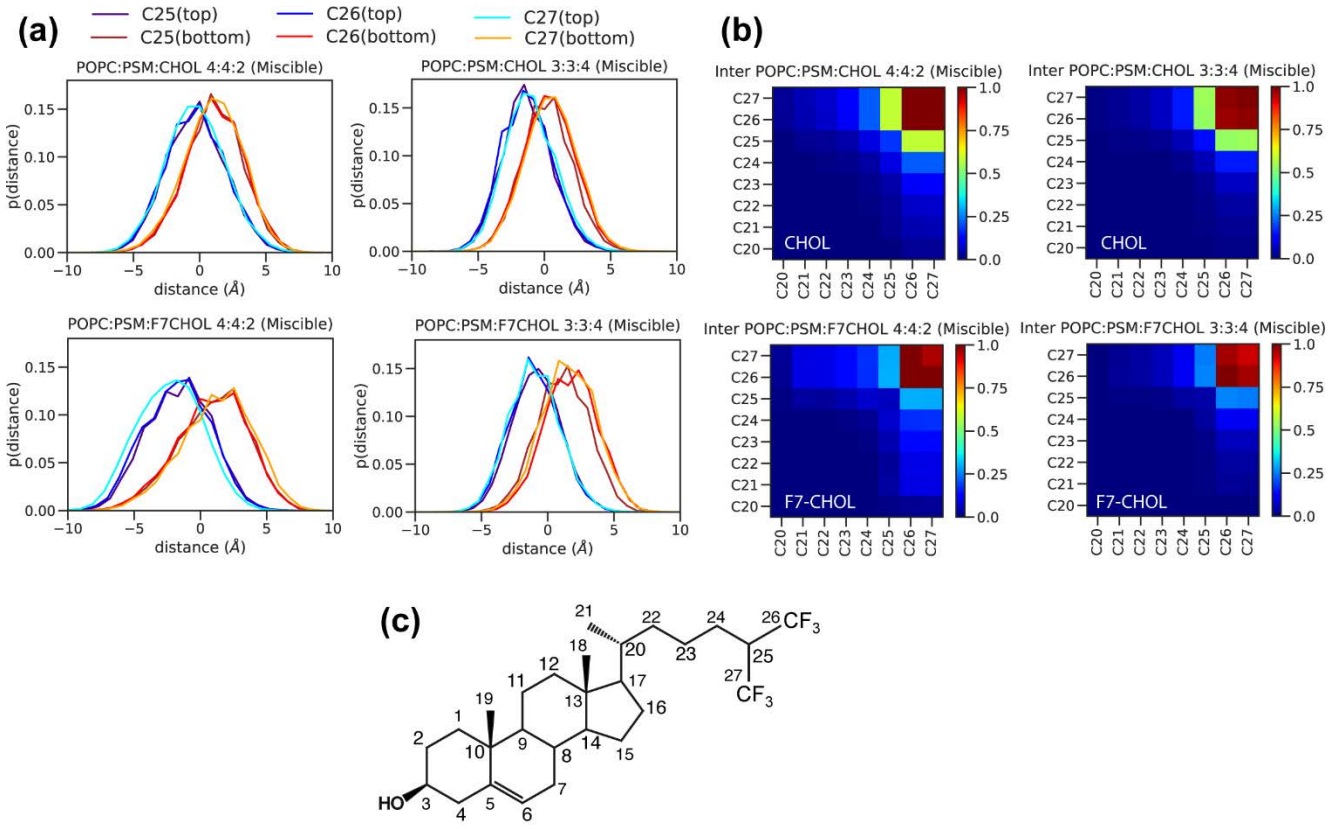

Figure S8. Chain-heptafluorinated cholesterol shows the same structure as hydrogenated cholesterol in lipid membranes. (a) Z-axial position distributions of CHOL C25, C26 and C27 atoms in hydrogenated cholesterol (top row) and F7-cholesterol (bottom row). (b) CHOL-CHOL contact maps in membranes containing non-fluorinated cholesterol (top row) and fluorinated cholesterol (bottom row). (c) Structure of 25,26,26,26,27,27,27-heptafluorocholesterol (F7-CHOL) with standard carbon numbering.

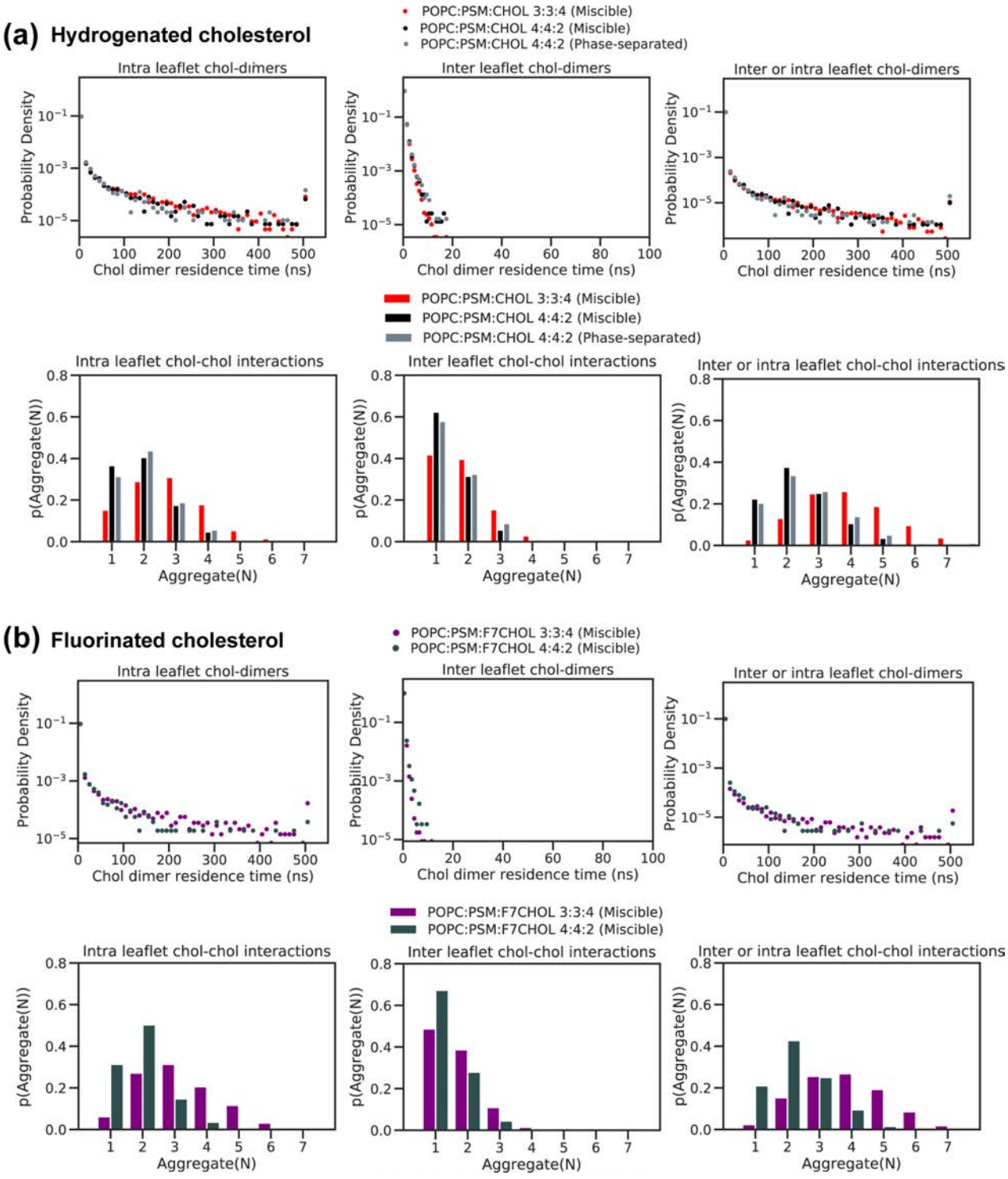

Figure S9. Hydrogenated and fluorinated cholesterols show similar dimer residence times and cluster size distributions in POPC : PSM : CHOL membranes. (a) Hydrogenated CHOL dimer residence times and cluster sizes. (b) Fluorinated CHOL dimer residence times and cluster sizes. Left column: intra-leaflet dimers. Middle column: inter-leaflet dimers. Right column: all forms of dimers.

References

1. Ounjian, J.; Bukiya, A. N.; Rosenhouse-Dantsker, A., Molecular Determinants of Cholesterol Binding to Soluble and Transmembrane Protein Domains. *Adv. Exp. Med. Biol.* **2019,** *1135*, 47-66.